Dynamics of Marine Cloud Layers: Computer Simulation and Experimental Verification

Final Technical Report
Grant No.: N00014-96-1-0973

Submitted to:
Office of Naval Research (Code 322MM)
Arlington, VA 22217

Submitted by:
University of the District of Columbia
Washington, DC 20008-1174

Prepared by:
Joseph Chi, Ph.D., P.E.
Professor of Mechanical Engineering

UDC Report Number:
N973-05

December 1998

Dynamics of Marine Cloud Layers: Computer Simulation and Experimental Verification

Final Technical Report
Grant No.: N00014-96-1-0973

Submitted to:
Office of Naval Research (Code 322MM)
Arlington, VA 22217

Submitted by:
University of the District of Columbia
Washington, DC 20008-1174

Prepared by:
Joseph Chi, Ph.D., P.E.
Professor of Mechanical Engineering

UDC Report Number:
N973-05

December 1998

ABSTRACT

Goals of this research have been to identify physical processes that determine the dynamics of the marine cloud layers and to quantify roles of turbulence, convection and thermal radiation that play in formation, dissipation and stability of the marine cloud layers. And immediate objectives of the research are to advance turbulence models, use efficient numerical schemes, develop computer simulation programs, simulate the marine cloud layers and compare computer results with published experimental data on the marine cloud layers so as to yield insights into the cloud's physical processes.

For these objectives, two theoretical models, using the second-order-turbulence closure and the large-eddy simulation (LES), respectively, have been developed. In addition, efforts have been made to develop a hybrid model that is based upon a framework of the LES model but uses turbulence values predicted by a second-order-closure model. This hybrid model preserves details of turbulence but eliminates the need of continuous evaluation of the multi dimensional turbulence equations. The model will improve simulation efficiency and conserve computational resources. An evaluation of the model has shown excellent agreement between simulation results with relevant experimental data retrieved from reliable web site resources.

In this report, a progressive development of the second-order-closure, LES and hybrid turbulence models for simulation of the marine cloud layers is described and a comparison of theoretical results with experimental data is presented to yield better insights into the cloud's physical processes.

TABLE OF CONTENTS

1. INTRODUCTION

Goals of this research have been to identify physical processes that determine the dynamics of the marine cloud layers and to quantify roles of turbulence, convection and thermal radiation that play in formation, dissipation and stability of the marine cloud layers. And immediate objectives of the research are to advance turbulence models, use efficient numerical schemes, develop computer simulation programs, simulate the marine cloud layers and compare theoretical results with published experimental data on the marine cloud layers so as to yield insights into the cloud's physical processes.

Studying the multi dimensional cloud layers requires a turbulence model that permits high-resolution simulation of turbulence of different scales and domain sizes. For high resolution, detailed second-order-closure model of turbulence may be used, and for calculation efficiency, the large-eddy-simulation (LES) model may be developed. Two computer simulation programs, using the second-order-closure model (Chi, 1996 and 1998a) and the LES model (Chi, 1998b), respectively, have been developed under this research effort. Additional efforts have been made to develop a hybrid model that is based upon a framework of the LES model but uses turbulence values predicted by a second-order-closure model. In addition, confidence in the simulation model is established by comparing simulation results with experimental data retrieved from reliable web site resources.

In this report, a progressive development of the second-order-closure, LES and hybrid turbulence models for simulation of the marine cloud layers will be documented first. Numerical experiments will be carried out to examine calculation efficiencies and characteristics of the marine cloud layers. Experience in tracking relevant experimental data from reliable web site resources will be described. To increase insight into the marine cloud layers, the computer simulation results are

compared with experimental data.

2. THEORETICAL MODELS FOR THE MARINE CLOUD LAYERS

For high resolution, a detailed second-order-closure model of turbulence has been developed. For calculation efficiency, a LES model has been developed. Details of these models have been reported in several papers by the author (Chi, 1996, 1998a, and 1998b). For ready references, reprints of these three papers are appended to the report. In addition, a hybrid turbulence model that is built upon a framework of the LES model but uses turbulence values predicted by a second-order-closure model has been used to predict stability of multi dimensional marine cloud layers. This hybrid model preserves details of turbulence but eliminates the need of evaluating the multi dimensional turbulence equations, and It improves prediction efficiency and conserve computational resources. In addition, prediction results have been shown in excellent agreement with relevant experimental data retrieved from reliable web site resources. Presented below in Section 2.1 is a second-order-closure model for calculating the turbulence values and in Section 2.2 is the framework of a LES model. In Section 2.3, a hybrid model that is based upon the LES framework but uses the second-order-closure turbulence values is described to predict stability of the marine cloud layers.

2.1 A Second-Order-Closure Model of Turbulence

When these assumptions are made: (1) vertical coordinate z is in the dominant direction of turbulent mixing of atmospheric air, (2) at far above a sea surface, the geostrophic balance is maintained, (3) velocity and temperature of vapor and liquid moisture are in equilibrium, and (4) Boussinesq approximations are used, the conservation equations for momentum, enthalpy and total moisture of atmospheric air can be written as:

$$\frac{\partial U}{\partial t} = f(V - V_g) - \frac{\partial uw}{\partial z} - W\frac{\partial U}{\partial z} \tag{1}$$

$$\frac{\partial V}{\partial t} = f(U_g - U) - \frac{\partial vw}{\partial z} - W\frac{\partial V}{\partial z} \tag{2}$$

$$\frac{\partial \Theta}{\partial t} = -W\frac{\partial \Theta}{\partial z} - \frac{\partial w\theta}{\partial z} - \frac{1}{\rho C_p}\frac{\partial F_R}{\partial z} \tag{3}$$

$$\frac{\partial \Omega}{\partial t} = -W\frac{\partial \Omega}{\partial z} - \frac{\partial w\omega}{\partial z} \tag{4}$$

where the upper-case dependent variables represent the mean fields and the corresponding lower-case variables represent turbulent fluctuations of the same variables. Thus, U, V and W are mean velocity components in the x, y and z directions and at the time t. (U_g, V_g) are geostrophic wind components in (x,y) directions. Θ is the mean moist-air potential temperature which is defined as $[T\text{-}T_o + (gz + L\Omega_v)/C_p]$, and Ω the mean total moisture mixing ratio which is defined as $(\Omega_v + \Omega_l)$. L is the water latent heat of vaporization, C_p the constant pressure specific heat, T the temperature, T_o the referenced temperature at z equal to zero, Ω_v the water vapor mixing ratio, Ω_l the liquid water mixing ratio, g the gravitational acceleration, f the Coriolis parameter, Θ_v the virtual dry potential temperature which is defined as $[T(1 + 1.609\Theta_v\text{-}\Omega)\text{-}T_o + gz/C_p]$, ϱ the standard density, ν the kinematic viscosity, and β the buoyancy coefficient, The second-order correlations in these equations represent the mean turbulent fluxes of momentum, enthalpy and moisture fluxes.

Using the second-order-closure assumption (Mellor and Yamada, 1974 and Moeng and Arakawa, 1980), transport equations for calculating the turbulent fluxes may be written as follows:

$$\frac{\partial u^2}{\partial t}=\frac{\partial}{\partial z}(Aq\lambda\frac{\partial u^2}{\partial z})-2\overline{uw}\frac{\partial U}{\partial z}-B\frac{q}{\lambda}(\overline{u^2}-\frac{q^2}{3})-D\frac{q^3}{3\lambda} \tag{5}$$

$$\frac{\partial v^2}{\partial t}=\frac{\partial}{\partial z}(Aq\lambda\frac{\partial v^2}{\partial z})-2\overline{vw}\frac{\partial V}{\partial z}-B\frac{q}{\lambda}(\overline{v^2}-\frac{q^2}{3})-D\frac{q^3}{3\lambda} \tag{6}$$

$$\frac{\partial w^2}{\partial t}=\frac{\partial}{\partial z}(3Aq\lambda\frac{\partial w^2}{\partial z})+2\beta\overline{w\theta}_v-B\frac{q}{\lambda}(\overline{w^2}-\frac{q^2}{3})-D\frac{q^3}{3\lambda} \tag{7}$$

$$\frac{uw}{\partial t}=\frac{\partial}{\partial z}(2Aq\lambda\frac{\partial uw}{\partial z})+\beta g\overline{u\theta}_v-(\overline{w^2}-C\overline{q^2})\frac{\partial U}{\partial z}-B\frac{q}{\lambda}\overline{u} \tag{8}$$

$$\frac{\partial vw}{\partial t}=\frac{\partial}{\partial z}(2Aq\lambda\frac{\partial vw}{\partial z})+\beta g\overline{v\theta}_v-(\overline{w^2}-C\overline{q^2})\frac{\partial V}{\partial z}-B\frac{q}{\lambda}\overline{v} \tag{9}$$

$$\frac{\partial u\theta}{\partial t}=\frac{\partial}{\partial z}(Aq\lambda\frac{\partial u\theta}{\partial z})-\overline{uw}\frac{\partial \Theta}{\partial z}-\overline{w\theta}\frac{\partial U}{\partial z}-E\frac{q}{\lambda}\overline{u\theta} \tag{10}$$

$$\frac{\partial v\theta}{\partial t}=\frac{\partial}{\partial z}(Aq\lambda\frac{\partial v\theta}{\partial z})-\overline{vw}\frac{\partial \Theta}{\partial z}-\overline{w\theta}\frac{\partial V}{\partial z}-E\frac{q}{\lambda}\overline{v\theta} \tag{11}$$

$$\frac{\partial w\theta}{\partial t}=\frac{\partial}{\partial z}(2Aq\lambda\frac{\partial w\theta}{\partial z})-\overline{w^2}\frac{\partial \Theta}{\partial z}+\beta g\overline{\theta\theta}_v-E\frac{q}{\lambda}\overline{w\theta} \tag{12}$$

$$\frac{\partial \theta^2}{\partial t}=\frac{\partial}{\partial z}(Aq\lambda\frac{\partial \theta^2}{\partial z})-2\overline{w\theta}\frac{\partial \Theta}{\partial z}-F\frac{q}{\lambda}\overline{\theta^2} \tag{13}$$

$$\frac{\partial u\omega}{\partial t}=\frac{\partial}{\partial z}(Aq\lambda\frac{\partial u\omega}{\partial z})-\overline{uw}\frac{\partial \Omega}{\partial z}-\overline{w\omega}\frac{\partial U}{\partial z}-E\frac{q}{\lambda}\overline{u\omega} \tag{14}$$

$$\frac{\partial \overline{v\omega}}{\partial t} = \frac{\partial}{\partial z}(Aq\lambda \frac{\partial \overline{v\omega}}{\partial z}) - \overline{vw}\frac{\partial \Omega}{\partial z} - \overline{w\omega}\frac{\partial V}{\partial z} - E\frac{q}{\lambda}\overline{v\omega} \tag{15}$$

$$\frac{\partial \overline{w\omega}}{\partial t} = \frac{\partial}{\partial z}(2Aq\lambda \frac{\partial \overline{w\omega}}{\partial z}) - \overline{w^2}\frac{\partial \Omega}{\partial z} + \beta g\overline{\omega\theta_v} - E\frac{q}{\lambda}\overline{w\omega} \tag{16}$$

$$\frac{\partial \overline{\omega^2}}{\partial t} = \frac{\partial}{\partial z}(Aq\lambda \frac{\partial \overline{\omega^2}}{\partial z}) - 2\overline{w\omega}\frac{\partial \Omega}{\partial z} - F\frac{q}{\lambda}\overline{\omega^2} \tag{17}$$

$$\frac{\partial \overline{\theta\omega}}{\partial t} = \frac{\partial}{\partial z}(Aq\lambda \frac{\partial \overline{\theta\omega}}{\partial z}) - \overline{w\omega}\frac{\partial \Theta}{\partial z} - \overline{w\theta}\frac{\partial \Omega}{\partial z} - F\frac{q}{\lambda}\overline{\theta\omega} \tag{18}$$

In equations 5 through 18, the time-derivative terms on the left-hand side model the transient variation of turbulence correlations. The second-order derivative terms on the right-hand side model turbulent diffusion. While the production of turbulence due to buoyancy is modeled by terms with buoyant coefficient β, the production of turbulence due to friction is modeled by products of second-order correlations and gradients of mean variables. Terms with coefficients B, C, E and F represent the turbulent redistribution. The characteristic length scale λ is equal to the value of the Blackadar's or the diffusion-length scale - λ_B or λ_D - whichever is the smallest. Turbulent dissipation is modeled by terms with coefficient D. Coefficients κ, A, B, C, D, E and F have been determined semi-empirically (Chi, 1994), having the values equal to 0.35, 0.21, 0.46, 0.053, 0.132, 0.44, and 0.23, respectively. Numerical procedures and computer programs have been developed to solve equations 1 through 18 with appropriate boundary conditions (Chi, 1996 and 1998a). Prediction results using the second-order-closure model will be presented and discussed in Section 4.1 of this report.

2.2 A LES Model for Marine Cloud Layers

When these assumptions are made: (1) the Coriolis force is negligible, (2) velocity and temperature of vapor and liquid moisture are in equilibrium, and (3) Boussinesq approximations are used, the conservation equations for momentum, enthalpy, total moisture and turbulent energy of atmospheric air can be written as:

$$\frac{\partial U}{\partial t}=2\frac{\partial}{\partial x}(K_m\frac{\partial U}{\partial x})+\frac{\partial}{\partial z}[K_m(\frac{\partial U}{\partial z}+\frac{\partial W}{\partial x})]-U\frac{\partial U}{\partial x}-W\frac{\partial U}{\partial z}-\frac{1}{\rho_o}\frac{\partial P}{\partial z} \tag{19}$$

$$\frac{\partial W}{\partial t}=\frac{\partial}{\partial x}[K_m(\frac{\partial U}{\partial z}+\frac{\partial W}{\partial x})]+2\frac{\partial}{\partial z}(K_m\frac{\partial W}{\partial Z})+\beta g(\Theta-\Theta_o)-U\frac{\partial W}{\partial x}-W\frac{\partial W}{\partial z}-\frac{1}{\rho_o}\frac{\partial P}{\partial z} \tag{20}$$

$$\frac{\partial \Theta}{\partial t}=\frac{\partial}{\partial x}(K_\theta\frac{\partial \Theta}{\partial x})+\frac{\partial}{\partial z}(K_\theta\frac{\partial \Theta}{\partial z})-U\frac{\partial \Theta}{\partial x}-W\frac{\partial \Theta}{\partial z} \tag{21}$$

$$\frac{\partial \Omega}{\partial t}=\frac{\partial}{\partial x}(K_\omega\frac{\partial \Omega}{\partial x})+\frac{\partial}{\partial z}(K_\omega\frac{\partial \Omega}{\partial z})-U\frac{\partial \Omega}{\partial x}-W\frac{\partial \Omega}{\partial z} \tag{22}$$

$$\frac{\partial U}{\partial x}+\frac{\partial W}{\partial z}=0 \tag{23}$$

$$\frac{\partial E}{\partial t}=-[U\frac{\partial E}{\partial x}+W\frac{\partial E}{\partial z}]+\frac{\partial}{\partial x}[K_E\frac{\partial E}{\partial x}]+\frac{\partial}{\partial z}[K_E\frac{\partial E}{\partial z}]+[-\frac{\beta}{\theta_o}\frac{\partial \theta_v}{\partial z}+2K_m(\frac{\partial U}{\partial x})^2 +K_m(\frac{\partial U}{\partial z}+\frac{\partial W}{\partial x})^2+2K_m(\frac{\partial W}{\partial z})^2]-\epsilon \tag{24}$$

In above equations, E is the turbulent energy defined as $q^2/2$, and the buoyancy terms associated with the virtual dry potential temperature Θ_v have been defined as follows:

$$\frac{\partial \Theta_v}{\partial z}=\frac{\partial \Theta}{\partial z}+(0.609\xi-1)\frac{L}{C_p}\frac{\partial \Omega}{\partial z}\quad For\ Clear\ Air\ Layers \tag{25}$$

$$\Theta_v = T(1+1.609\Omega_v - \Omega) + \frac{gz}{C_p} \tag{26}$$

$$\frac{\Theta_v}{z} = \frac{1+1.609\xi\eta}{1+\eta}\frac{\partial\Theta}{\partial z} - \xi\frac{L}{C_p}\frac{\partial\Omega}{\partial z} \quad \textit{For Cloudy Air Laye} \tag{27}$$

The rate of dissipation within the grid volume and the subgrid eddy coefficient may be parameterized through

$$\epsilon = 0.19E^{3/2}/\lambda \tag{28}$$

and the eddy diffusivity coefficients have been defined as follows:

$$K_m = 0.58E^{1/2}\lambda \tag{29}$$

$$K_\theta = \frac{K_m}{\sigma_\theta}(1+\frac{2\lambda}{\lambda_S}) \tag{30}$$

$$K_\omega = \frac{K_m}{\sigma_\omega}(1+\frac{2\lambda}{\lambda_S}) \tag{31}$$

$$K_{ea} = \frac{K_m}{\sigma_e} \tag{32}$$

where λ is a minimum of the Blackadar's length λ_B, diffusion length λ_D, resolvable length scale λ_S:

$$\lambda_B = \frac{0.35z\delta}{\delta+3.5z} \tag{33}$$

$$\lambda_D = 0.75(\frac{e\theta\partial z}{g\partial\theta_v})^{1/2} \tag{34}$$

$$\lambda_S=(\Delta x\Delta x\Delta z)^{1/3} \tag{35}$$

$$\delta=\frac{\int_0^\infty E^{1/2}zdz}{\int_0^\infty E^{1/2}dz} \tag{36}$$

And the turbulent Prandtl numbers for enthalpy and moisture diffusion (σ_θ and σ_ω) are both equal to 0.75. Numerical procedures and computer programs have been developed to solve equations 19 through 31 with appropriate boundary conditions (Chi, 1998b). Prediction results using the LES model will be presented and discussed Section 4.2 of this report.

In Section 2.3, a hybrid model that retains high resolution with the second-order-closure model described in Section 2.1 and calculation efficiency with the LES model described in Section 2.2 will now be presented.

2.3 A Hybrid Turbulence Model for Marine Cloud Layers

Second- and higher-order turbulent models have succeeded in advancing theoretical understanding of the marine cloud layers. Complexity of those models often makes long-term simulation of the cloud layer over an extensive period prohibitively expensive. A hybrid model that retains calculation efficiency of the LES model and turbulence details of the second-order-closure model has been developed. The hybrid model uses Equations 19 through 23 from the LES model for conservations of momentum, enthalpy, moisture and mass, respectively:

$$\frac{\partial U}{\partial t}=2\frac{\partial}{\partial x}(K_m\frac{\partial U}{\partial x})+\frac{\partial}{\partial z}[K_m(\frac{\partial U}{\partial z}+\frac{\partial W}{\partial x})]-U\frac{\partial U}{\partial x}-W\frac{\partial U}{\partial z}-\frac{1}{\rho_o}\frac{\partial P}{\partial z} \tag{19}$$

$$\frac{\partial W}{\partial t}=\frac{\partial}{\partial x}[K_m(\frac{\partial U}{\partial z}+\frac{\partial W}{\partial x})]+2\frac{\partial}{\partial z}(K_m\frac{\partial W}{\partial Z})+\beta g(\Theta-\Theta_o)-U\frac{\partial W}{\partial x}-W\frac{\partial W}{\partial z}-\frac{1}{\rho_o}\frac{\partial P}{\partial z} \tag{20}$$

$$\frac{\partial \Theta}{\partial t}=\frac{\partial}{\partial x}(K_\theta \frac{\partial \Theta}{\partial x})+\frac{\partial}{\partial z}(K_\theta \frac{\partial \Theta}{\partial z})-U\frac{\partial \Theta}{\partial x}-W\frac{\partial \Theta}{\partial z} \tag{21}$$

$$\frac{\partial \Omega}{\partial t}=\frac{\partial}{\partial x}(K_\omega \frac{\partial \Omega}{\partial x})+\frac{\partial}{\partial z}(K_\omega \frac{\partial \Omega}{\partial z})-U\frac{\partial \Omega}{\partial x}-W\frac{\partial \Omega}{\partial z} \tag{22}$$

$$\frac{\partial U}{\partial x}+\frac{\partial W}{\partial z}=0 \tag{23}$$

But, instead of the turbulent-kinetic-energy Equation 24, the second-order-closure model equations 1 through 18 will be used in evaluating the eddy-diffusivity-coefficient K values defined by Equations 29 through 32. Numerical Procedure and computer algorithms (described in Section 3 below) have been developed to evaluate the hybrid model. Prediction results using the hybrid model will be presented in Section 4.3 and verified by comparison with experimental data in Section 5.2.

3. NUMERICAL PROCEDURE AND COMPUTER ALGORITHM

The hybrid model presented in Section 2.3 uses the turbulence equations 1 through 18, the conservation equations 19 through 23, and the diffusivity coefficients defined by Equations 29 through 32. Numerical procedures and computer algorithms have been developed to simulate the marine cloud layers. It can be observed above that conservation and turbulence transport equations 1 through 23 described above can be written in the following general form:

$$\frac{\partial \alpha}{\partial t}+U\frac{\partial \alpha}{\partial x}+W\frac{\partial \alpha}{\partial z}=-\frac{\partial}{\partial x}(\Gamma\frac{\partial \alpha}{\partial x})-\frac{\partial}{\partial z}(\Gamma\frac{\partial \alpha}{\partial z})+\Phi \quad \textit{within Domain } \Lambda \tag{37}$$

The boundary and initial conditions may be written as:

$$\frac{\partial \alpha}{\partial n}+a\alpha+b=0, \quad \textit{On boundary} \tag{38}$$

$$\alpha(x,z,t=0)=\alpha_{\eta}(x,z), \quad \textit{At initial time zero} \tag{39}$$

In above equations, $\alpha(x,z,t)$ values are variable values of velocity components U and W, potential temperature Θ, and moisture mixing ratio Ω; $\phi(x,z,t)$ values are the source/sink strengths for α. Items in equation 37 describe the variables' time derivative, convection, diffusion and source/sink strength, respectively. 'a' and 'b' values in equation 38 are used to define the appropriate boundary conditions.

A finite-volume difference scheme (Patanka, 1980) was used for descritization of variables. The flow domain to be simulated was divided into small rectangular elements; shown in a figure below are examples of several such elements. It can be seen in the figure that variable values at node points of the elements are strategically located. The node point for velocity value is located in the middle of the rectangular edge and the node point for other variables is located in the center of the rectangular box.

A Figure Showing an Element with Neighboring Variables

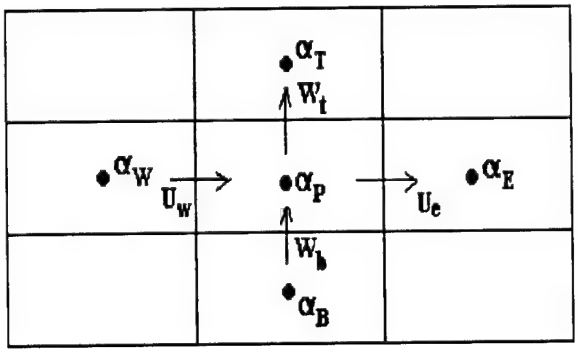

Using the velocity values and values of α shown in the figure and employing an upwind logic, the conservation law may be applied to obtain an expression for the value of α at the node point P in terms of the α-values at its neighboring node points:

$$a_P\alpha_P=a_E\alpha_E+a_W\alpha_W+a_T\alpha_T+a_B\alpha_B+b \tag{40}$$

where coefficient values 'a' and 'b' may be expressed in terms of the diffusion and flux parameters defined as follows:

$$a_E=\frac{K_e\Delta z}{\Delta x_e}+Max[-(U_e\Delta z),0] \tag{41}$$

$$a_W=\frac{K_w\Delta z}{\Delta x_w}+Max[(U_w\Delta z),0] \tag{42}$$

$$a_T=\frac{K_t\Delta x}{\Delta z_t}+Max[-(U_t\Delta x),0] \tag{43}$$

$$a_B=\frac{K_b\Delta x}{\Delta z_b}+Max[(U_b\Delta x),0] \tag{44}$$

$$a_P=a_E+a_W+a_T+a_B+\frac{\Delta x\Delta z}{\Delta t} \tag{45}$$

$$b=\phi_P\Delta x\Delta z \tag{46}$$

In addition, in solving U and W values using equation 40, the initial pressure values will have to be the estimated values; consequently, the equation 40 will yield initially approximate U_{app} and W_{app} values. Improved U and W values may be calculated from their approximate values using equations:

$$U_e=U_{e,app}+\frac{\Delta z}{a_P\rho_o}(P_P-P_E) \tag{47}$$

$$U_w=U_{w,app}+\frac{\Delta z}{a_P\rho_o}(P_w-P_P) \tag{48}$$

$$W_t = W_{t,app} + \frac{\Delta x}{a_P \rho_o}(P_P - P_T) \tag{49}$$

$$W_b = W_{b,app} + \frac{\Delta x}{a_P \rho_o}(P_b - P_P) \tag{50}$$

Substituting U and W values in equations 47 to 50 into the continuity equation 23 yields a set of linear equations for pressure values at the solution domain's node points; they may be used to solve for improved pressure values. So the process may be repeated to iterate alternatively for improved values of velocity, pressure and other variables at the node points.

Using the linear equations discussed above for variable values U, W, Θ, Ω, E and P at node points, a computer program has been written to simulate dynamics of the marine cloud layers.

4. COMPUTER SIMULATION RESULTS

4.1 Second-Order-Closure Model Simulation Results

The second-order-closure model of turbulence described in Section 2.1 has been used to predict transient exchange of moisture in the sea/air interface, mixing of moisture in the marine atmosphere, and formation of the cloud layer. Graphs plotted in figure 1 were reported in a previous paper written by the author (Chi, 1996); they were used as initial conditions for this study.

The initial conditions shown in figure 1 were obtained on the assumptions that the geostrophic wind in the x-direction was at 10m/s, and Coriolis parameter f is equal to 1.0×10^{-4} s^{-1}, the potential temperature was chosen to be well-mixed at 290K, and the total moisture mixing ratio corresponding to 100 percent relative humidity at top of the marine planetary boundary layer (MPBL). Just above the MPBL top at height equal to 1 kilometer, there was an inversion layer of 400-m thick, in which

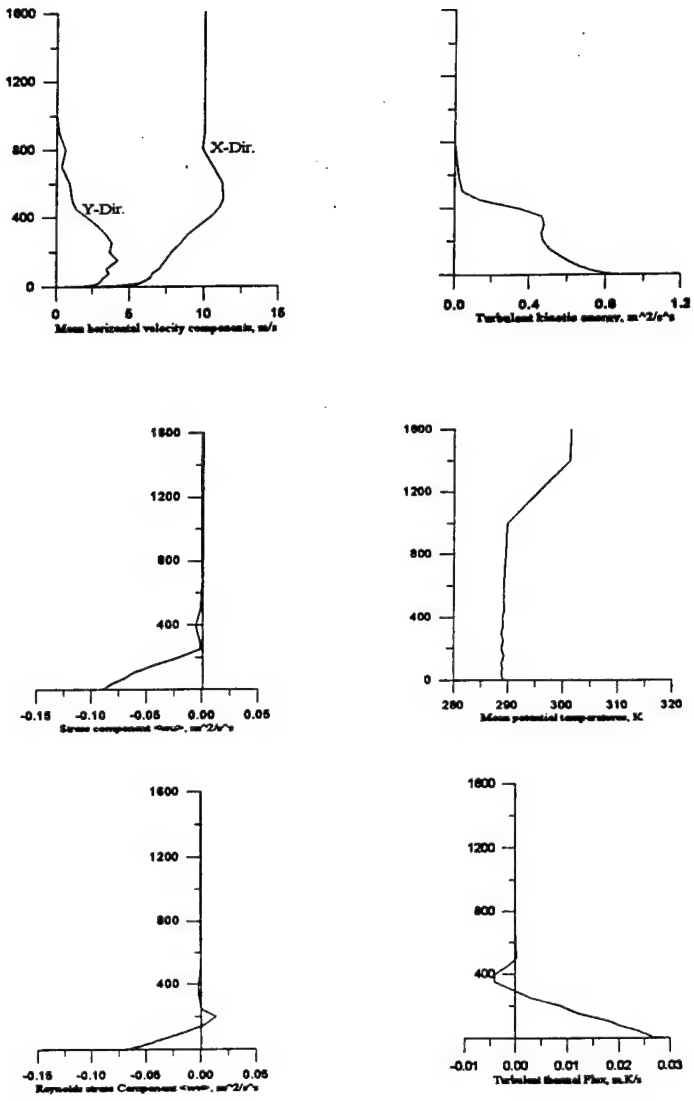

Fig. 1: Initial Velocity-Components and Potential-Temperature Values

temperature was increasing at 0.2 K/m and the moisture mixing ratio was decreasing at 0.008 g/kg.m, respectively. The sea-surface temperature was allowed to vary diurnally within the range of 280 to 290F. Conditions shown in figure 2 were for the instance when the sea surface was at 290 K.

For the simulation run using initial conditions shown in figure 1, it was assumed that the sea

surface temperature was raised abruptly to and then maintained at 298 K, and the air total moisture ratio at the sea surface was maintained at the saturation state. After simulation runs over a period of forty hours, a large body of data was generated. Plotted in figures 2 are predicted contours of temporal mean physical-property values of air in the marine atmosphere; plotted in figures 3 are predicted contours of Reynolds-stress and turbulent-flux values in the marine atmosphere. Many interesting characteristics of mixing in the simulation domain can be observed in these contours. Firstly, rapid interaction at the air/sea interface can be observed during the initial period of zero to 600 minutes. It is followed by a calmer development of the marine planetary boundary layer for about 600 minutes. Then, during the next 600 minutes transfer of enthalpy and moisture continues, as can be observed from the predicted contours of the turbulent thermal and moisture-flux values shown in figures 2C and 2D. Also, can be observed in Fig. 2D is the formation of cloud starting at the 200th minute, rapid deepening of the cloud layer during the second interval of 200 to 1200 minutes, and slower growth of the cloud layer during the period of 1200 to 1800 minutes. Finally, a steady state is established at around the 2400th minute.

Plotted in figures 4 and 5 are the predicted steady-state conditions at the end of the simulation period of the 40th hour. The graphs shown in figure 4 can be compared with those in figure 1 for the initial conditions. Changes that have been made during these forty hours can be observed. Warm and moist air at a sea surface has resulted in an unstable mixing layer. Variations of both the mean-quantity and the turbulent-flux profiles can be observed in figure 4. Specifically, if mean horizontal velocity components plotted in figures 1A and turbulent kinetic energy values plotted in figure 1B are compared with those corresponding values plotted in figure 4A and 4H, thickening of the unstable boundary layer due to intense turbulent exchange can be observed in figure 4A and 4H.

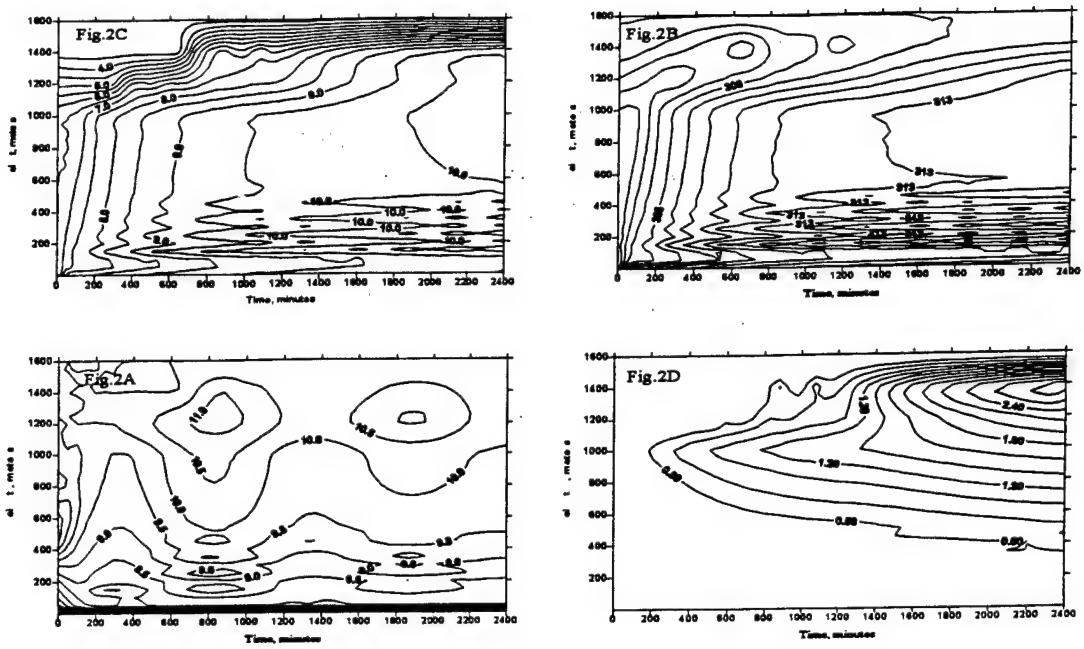

Fig. 2: Predicted Contours of Mean Atmospheric Quantities
2A - Mean Wind Velocity, m/s, 2B - Mean Potential Temperature, K,
2C - Mean total moisture mixing ratio, g/kg, 2D - Mean liquid moisture mixing ratio, g/kg

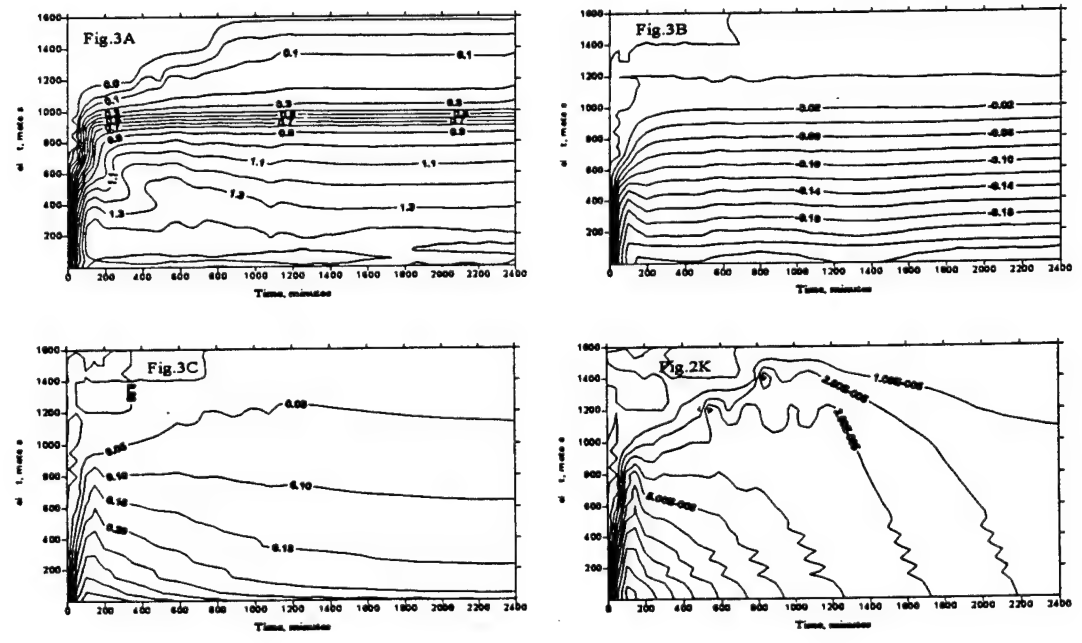

Fig. 3: Predicted Contours of Turbulent Fluxes
3A - Turbulent kinetic energy, m^2/s^2, 3B - Principal Reynolds stress, m^2/s^2
3C - Turbulent thermal flux, m.K/s, 3D - Turbulent moisture flux, m.kg/kg.s^3

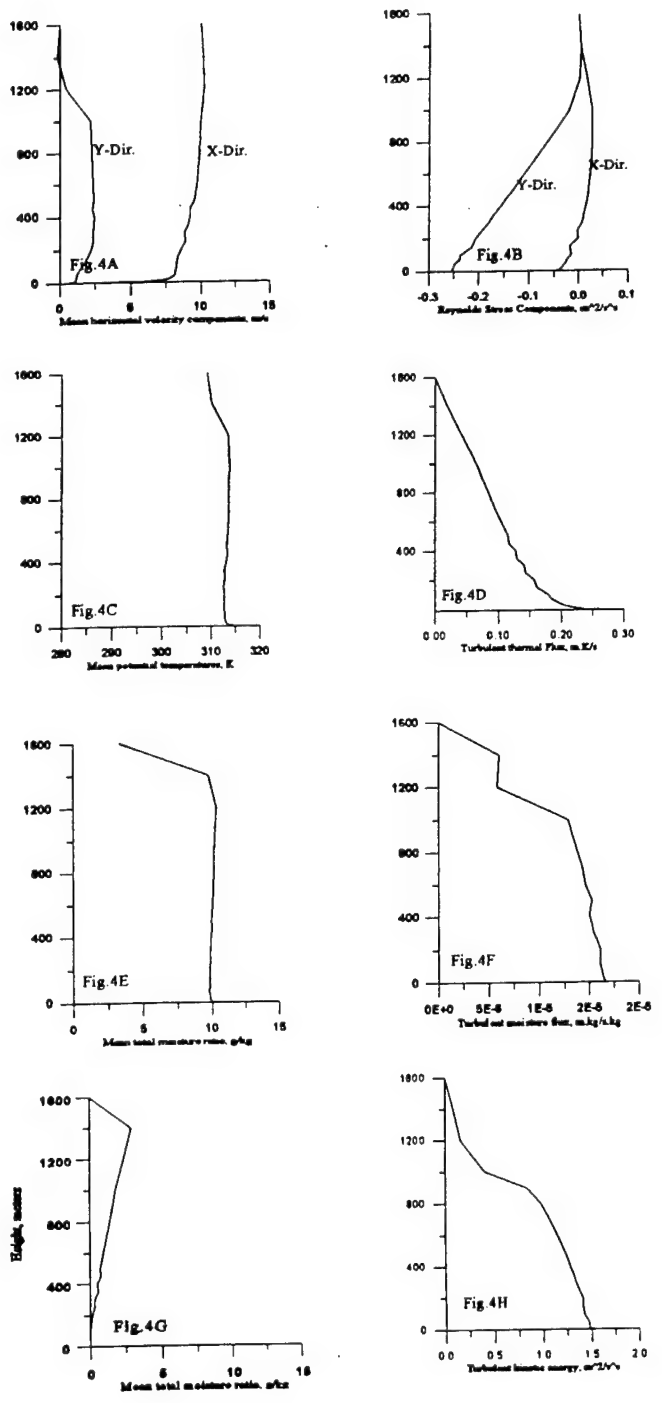

Fig. 4: Predicted Mean Quantities and Turbulent Fluxes
4A - Mean velocity; 4B - Reynolds stress;
4C - Potential temperature; 4D - Thermal flux;
4E - Total moisture ratio; 4F - Moisture flux;
4G - Liquid moisture ratio; 4H - Turbulent energy.

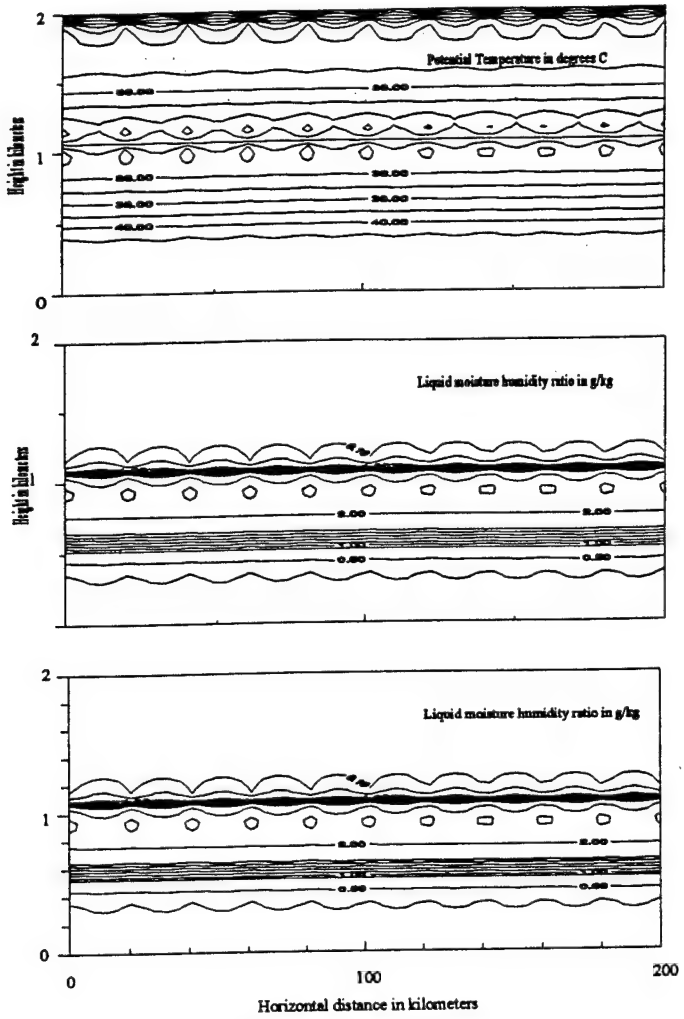

Fig. 5: Initial steady state at the zeroth hour

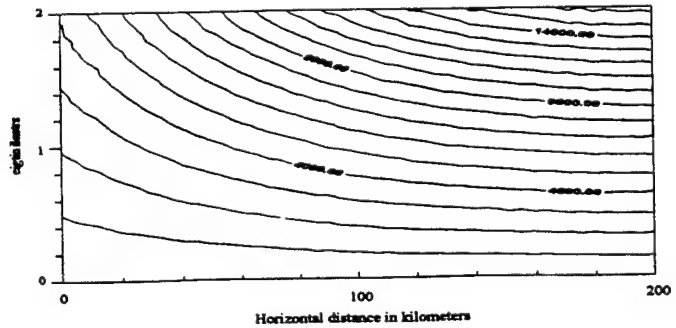

Fig. 6: Contours of superposed stream functions with entrainment at the top

4.2 LES Model Simulation Results

The LES model presented in Section 2.2 has been used to study stability of the marine cloud layers. Graphs plotted in figure 4 and 5 predicted by a second-order-closure model presented in Section 4.1 above can be used as a set of initial values in this numerical experiment. It may be noted that solutions for this set of graphs were obtained by using the main stream wind velocity U equal to 10 m/s. To investigate effects of cloud-top-warm-air entrainment on stability of the cloud layer shown in figure 5, a stream function shown in figure 6 will be superimposed to the main flow. In generating the stream function shown in figure 6, the top-down entrainment was assumed to be at a maximum rate of 6 cm/s is at the top-left corner and the rate was reduced sinusoidally to zero at the top-right corner. In addition, it is assumed that potential temperature of the entrained air is at five degrees centigrade higher than that of the cloud at the top.

Using the initial conditions and entrainment rates described above, a LED simulation computer program has been run. Shown in figure 5 are contours of the initial steady-state potential temperature values, total moisture mixing ratio values and liquid moisture Mixing values, respectively. Predicted dynamic responses of the cloud layer's liquid moisture content to the warm-air entrainment at the top are shown in figure 7. From snapshots shown in this figure of the cloud contours at different times (i.e., at half, one, five and ten hours from the start of the simulation run), dissipation of the cloud layer can be observed.

A comparison of this example with that presented in Section 4.1, it can be observed that the LES model is superior to the second-order-closure model in calculation efficiency. However, details of turbulence are lost in trading for this efficiency.

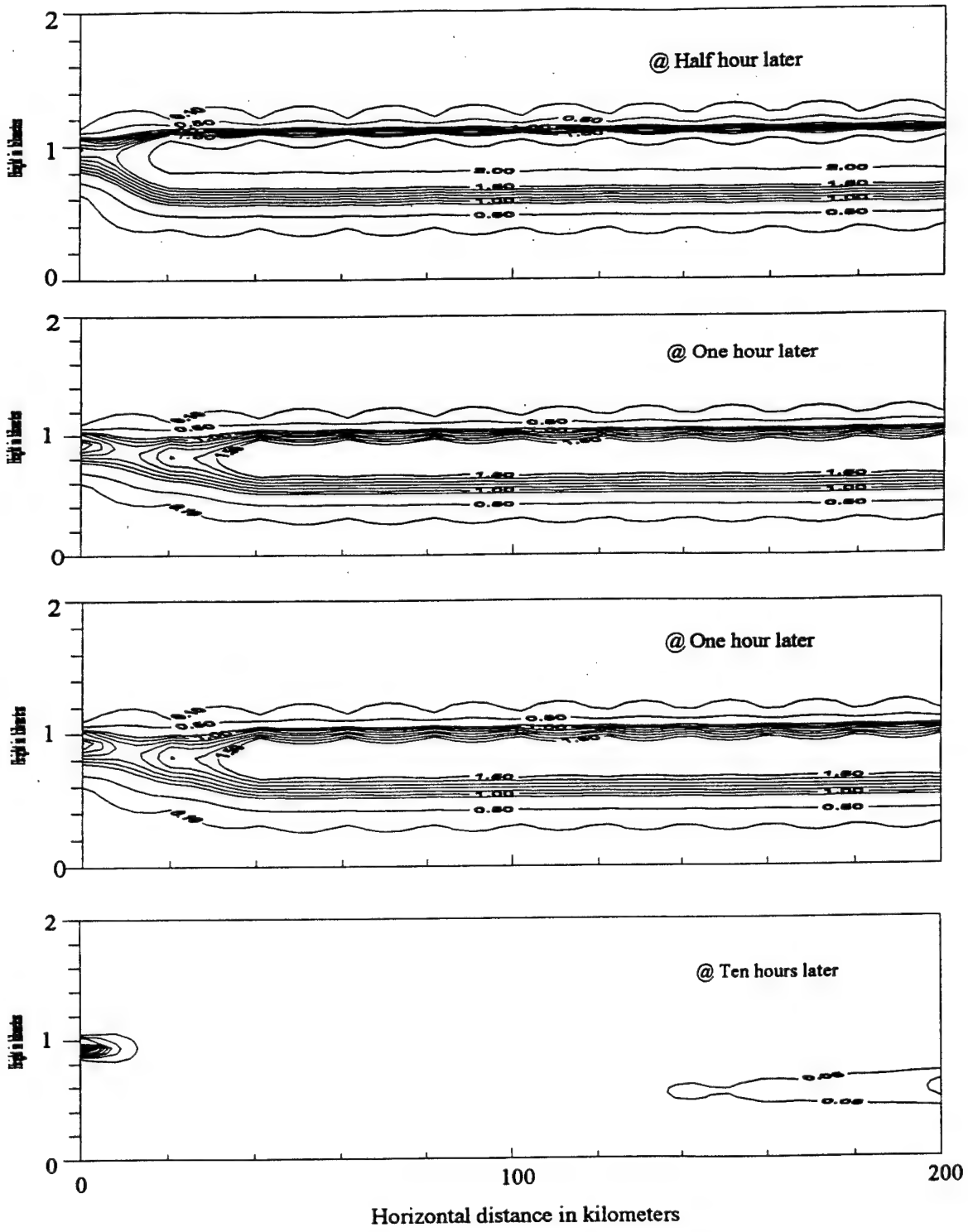

Fig. 7: Predicted effects of warm-air entrainment on the cloud stability
(Contours are for liquid-moisture mixing ratio in g/km)

4.3 Hybrid Model Simulation Results

In order to preserve details of the second-order-closure turbulence and calculation efficiencies of large-eddy simulation, a computer program using the hybrid model developed in section 2.3 has been written to study stability of the marine cloud layer. Numerous runs of the computer program have been made to simulate dynamic responses of marine cloud layers under a variety of conditions. To facilitate later comparison of simulation results with TOGA-COARE data (Tropical Ocean Global Atmosphere - Coupled Ocean Atmosphere Response Experiment) documented by Tao and Simpson (1993), Miller and Riddle (1994) and Lin and Johnson (1996), computer runs have been made with internet retrieved experimental stream-function and boundary-condition values as input data. As an example, figure 8 shows an initial experimental dataset for the stream-function values, and figure 9 shows snapshots of cloud profiles predicted by the hybrid model, at several different instances, starting from the zeroth hour to the 24th hour.

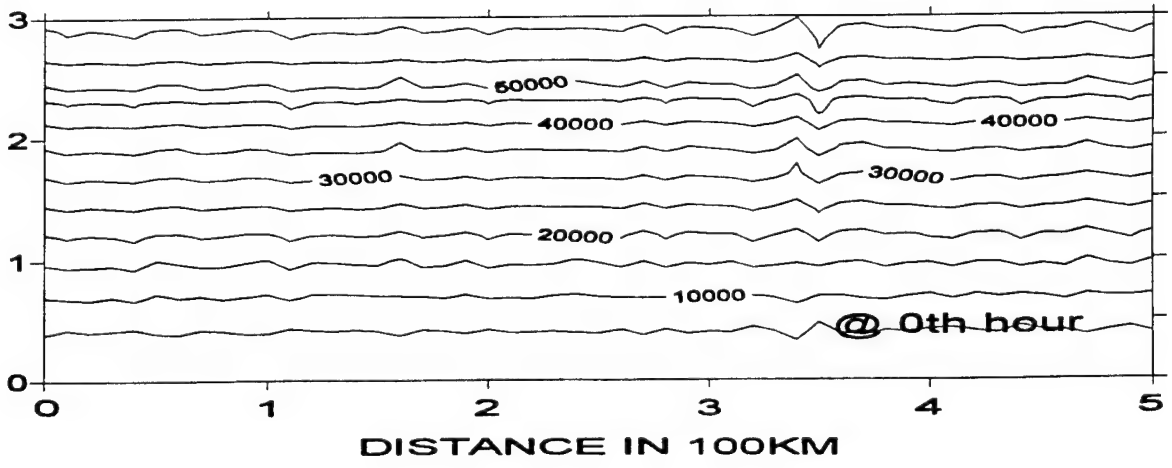

Fig. 8: Contours of a set of retrieved experimental stream function values

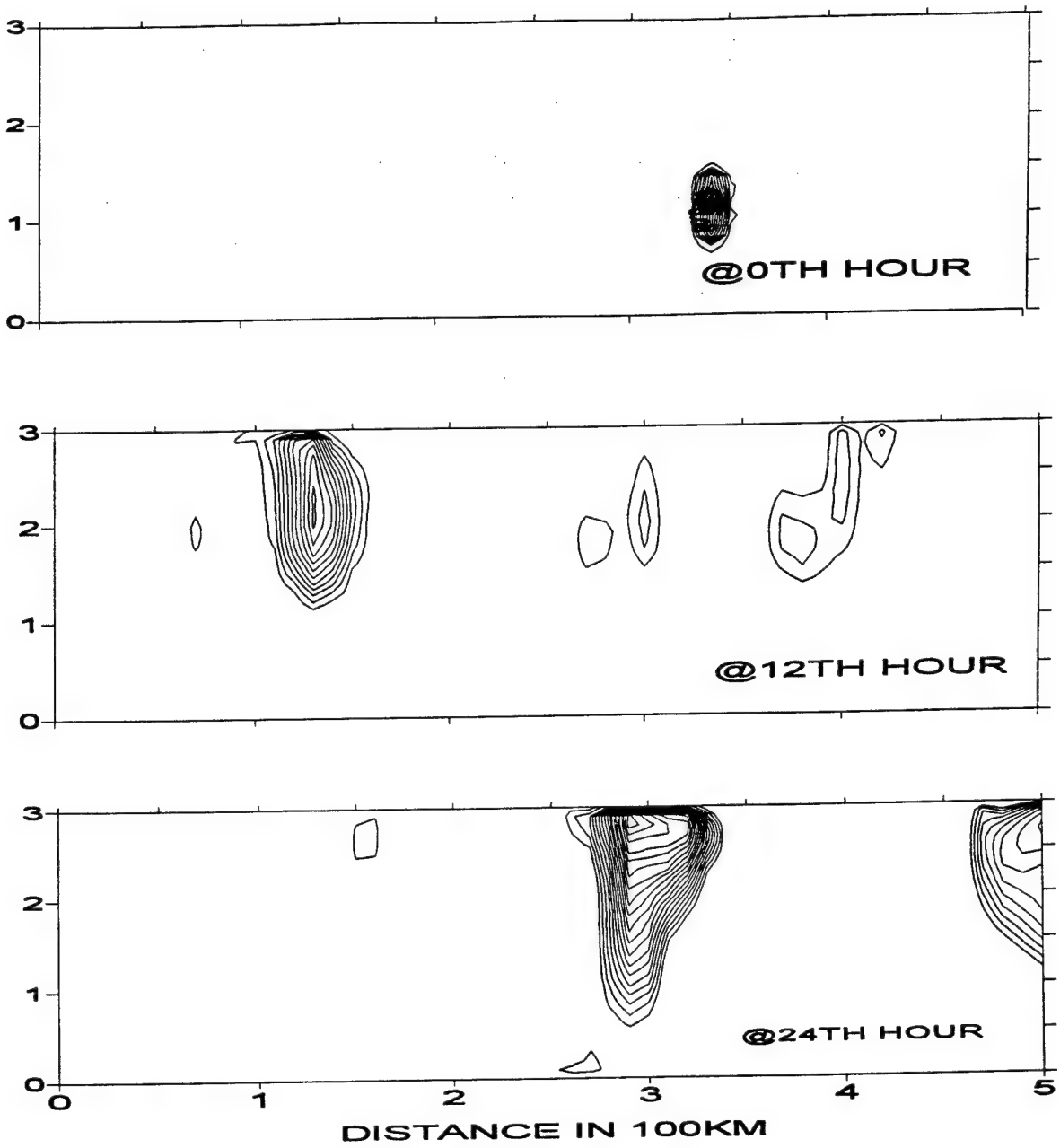

Fig. 9: Snapshots of cloud contours predicted by a hybrid model of turbulence
(Starting from an initial experimental dataset at the zeroth hour)

5. DATA TRACKING AND THEORETICAL VERIFICATION

5.1 Internet Atmospheric Data Tracking

Several data sources such as Goddard Cumulus Ensemble (GCE), GDACC (Goddard Distributive Active Archive Center), FIFI (First ISLCP Field Experiment) and TOGA-COARE (Tropical Ocean Global Atmosphere - Coupled Atmosphere Response Experiment) were reviewed to determine the time interval, grid size and altitude criteria. It was determined that we should secure data with time and grid intervals at six hours and one mile, respectively. Two sources of data TOGA-COARE (Webster and Lukas, 1992) and GCE (Tao, 1993) were then considered.

TOGA-COARE DATA: The scientific goals of COARE are to describe and understand: (1) the principal processes responsible for the coupling of the ocean and the atmosphere in the western Pacific warm-pool systems, (2) the principal atmospheric processes that organize convection in the warm-pool region, (3) the oceanic response to combined buoyancy and wind-stress forcing in the western Pacific warm- pool region, and (4) the multiple-scale interactions that extend the oceanic and atmospheric influence of the western Pacific warm-pool system to other regions and vice versa. To carry out the goals of TOGA COARE, three components of a major field experiment have been defined: interface, atmospheric, and oceanographic. The experimental design calls for a complex set of oceanographic and meteorological observations from a variety of platforms that carry out remote and in situ measurements. The resulting high-quality dataset is required for the calculation of the interfacial fluxes of heat, momentum and moisture, and to provide ground thruth for a wide range of remotely sensed variables for the calibration of satellite-derived algorithms. The ultimate objective of the COARE dataset is to improve air-sea interaction and boundary-layer parameterizations in models of the ocean and the atmosphere, and to validate coupled models.

Internet web-site data was used to review the data sets of TOGA-COARE. Several sites for data were reviewed. The web site, http://kiwi.atmos.colostate.edu/scm/toga-coare.html was found to contain mean data over the TOGA-COARE IFA region, which were thought appropriate for testing the model. Using FTP commands the data files were transferred to a main frame computer. Using uncompress command the compressed files were uncompressed and converted to ASCII files and transmitted to a UDC workstation via electronic mails. However, owing to their coarse grid sizes, higher resolution datasets are required for the model refinement.

GCE MODELS DATA: The Goddard Cumulus Ensemble Model (GCE) is maintained by Mesoscale Atmospheric Processes Branch (MAPB) at Goddard Space Flight Center (NASA/GSFC). Scientists in NASA/GSFC continuously maintain and upgrade the system (Tao and Simpson, 1993), and the GCE model is simulated and operated by GSFS system analysts and operators (Private communications). The GEC model may be used to interpolate experimental data with great degrees of accuracy. The following procedures were followed to obtain the data from both sources:

Super computer CRAY at NASA was used for obtaining, organizing, processing the data. The data files obtained in this process were transmitted to the UDC workstation via electronic mail. For GCE Model data, scientists at GSFC provided the author and his co-workers at UDC with the database and a Fortran program including a list of parameters via electronic mail. Fortran programs were further developed and modified the data into appropriate formats for the files. The data from GCE model were processed using the Fortran programs in UNIX environment. Then. They were transmitted to the UDC workstation in two stages.

The First-stage data transmitted included the following parameters:

parameter (nx=512,nz=22)

```
parameter (nhr=48)            ! number of hours model simulations (h)
parameter (interval=21600)    ! Interval to read in data (s)
parameter (ntimes=nhr*3600/interval)
real latent (nx,ntimes)       ! surface latent heat flux (W/m**2)
real p0 (nz)                  ! air pressure (mb)
real qcg(nx,nz,ntimes)        ! graupel mixing ratio (g/kg)
real qci(nx,nz,ntimes)        ! cloud ice mixing ratio (g/kg)
real qcl(nx,nz,ntimes)        ! cloud water mixing ratio (g/kg)
real qcs(nx,nz,ntimes)        ! snow mixing ratio (g/kg)
real qrn(nx,nz,ntimes)        ! rain water mixing ratio (g/kg)
real rad_lw(nx,nz,ntimes)     ! long wave radiative heating rate (K/hr)
real rad_sw(nx,nz,ntimes)     ! short wave radiative heating rate (K/hr)
real sensible(nx,ntimes)      ! surface sensible heat flux  (W/m**2)
real temp(nx,nz,ntimes)       ! air temperature (K)
real u(nx,nz,ntimes)          ! u-wind speed (m/s)
real v(nx,nz,ntimes)          ! v-wind speed (m/s)
real vap(nx,nz,ntimes)        ! water vapor mixing ratio (g/kg)
real w(nx,nz,ntimes)          ! w-wind speed (m/s)
real z1(nz)                   ! model grid height at z1 levels - for most variables here (m)
real z2(nz)                   ! model grid height at z2 levels - where 2 is (m)
```

nx=512 (512 miles, data grid = one mile)
nz=22 -> pressure levels
ntimes=32 (6-hrs intervals)

The Second-stage data transmitted included the following parameter:

```
real tke(nx,nz)               ! turbulent kinetic energy (cm*cm/s/s)
real du(nx,nz)                ! u-momentum turbulence rate (cm/s/s)
real dv(nx,nz)                ! v-momentum turbulence rate (cm/s/s)
real dw(nx,nz)                ! w-momentum turbulence rate (cm/s/s)
```

nz=22 -> pressure levels
ntimes=32 (6-hrs intervals)

The database obtained from the GCE model was large. Eight six-hours data were organized in eight different data files, each file containing one six-hour interval of data. The data files were transmitted via electronic mails.

DATA PRESENTATION: For graphic presentation, they were further decoded at UDC by several Fortran programs, and were translated into formats recognizable by data plotting software packages - Surfer and Grapher - which are available in the author's laboratory. Presented below are plotted sample data values over a domain with a height of 3-km and a horizontal distance of 500-km, and over a time period of 24 hours at 12-hours intervals:

- Contours of empirical wind flow stream functions values
- Contours of empirical total moisture mixing ratio values
- Contours of empirical liquid moisture mixing ratio values
- Sea/air interface sensible and latent heat flux values

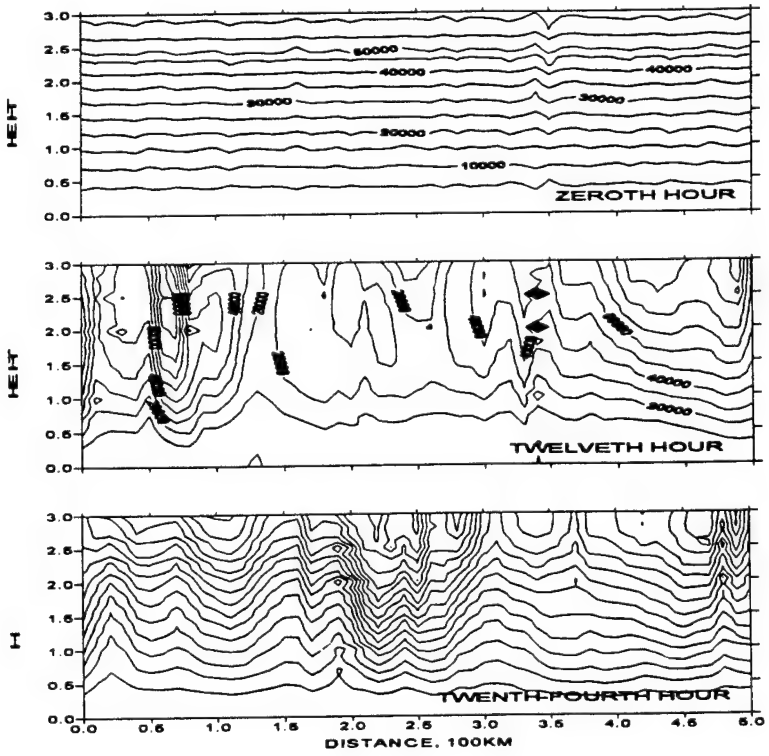

Fig. 10: Contours of experimental wind stream-function values

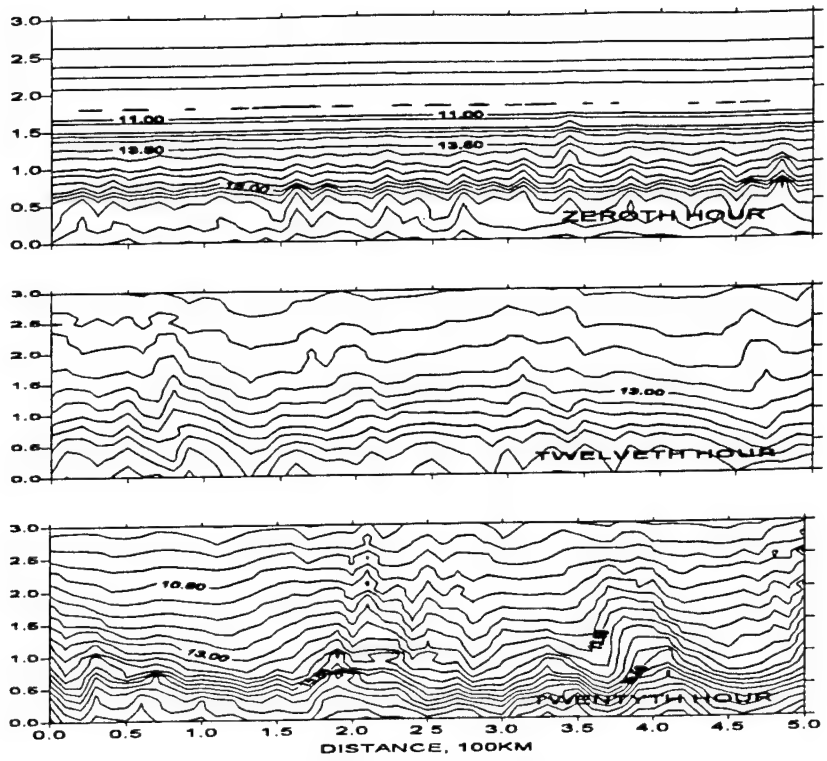

Fig. 11: Contours of experimental total moisture mixing ratio

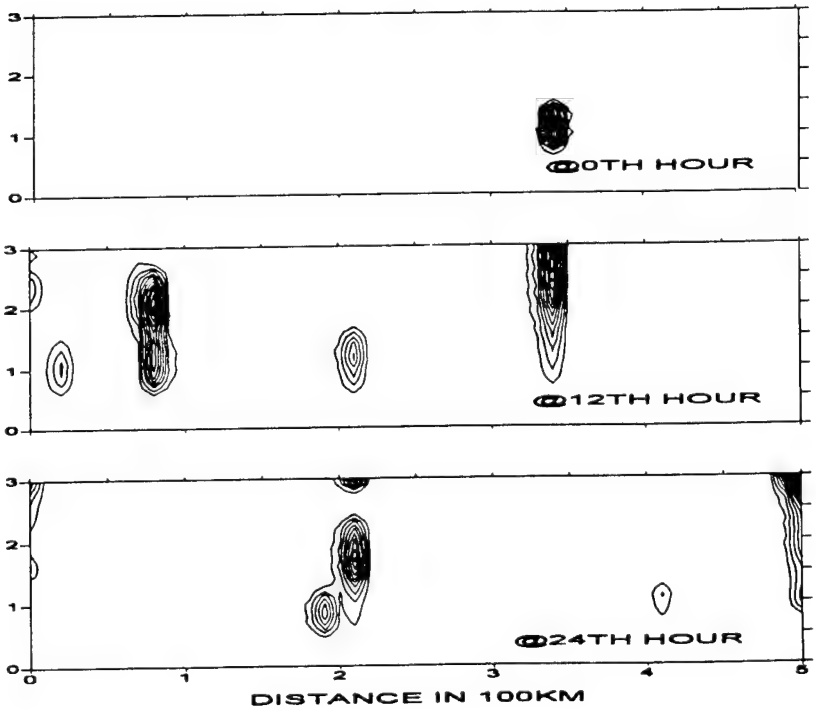

Fig. 12: Contours of empirical cloud profiles

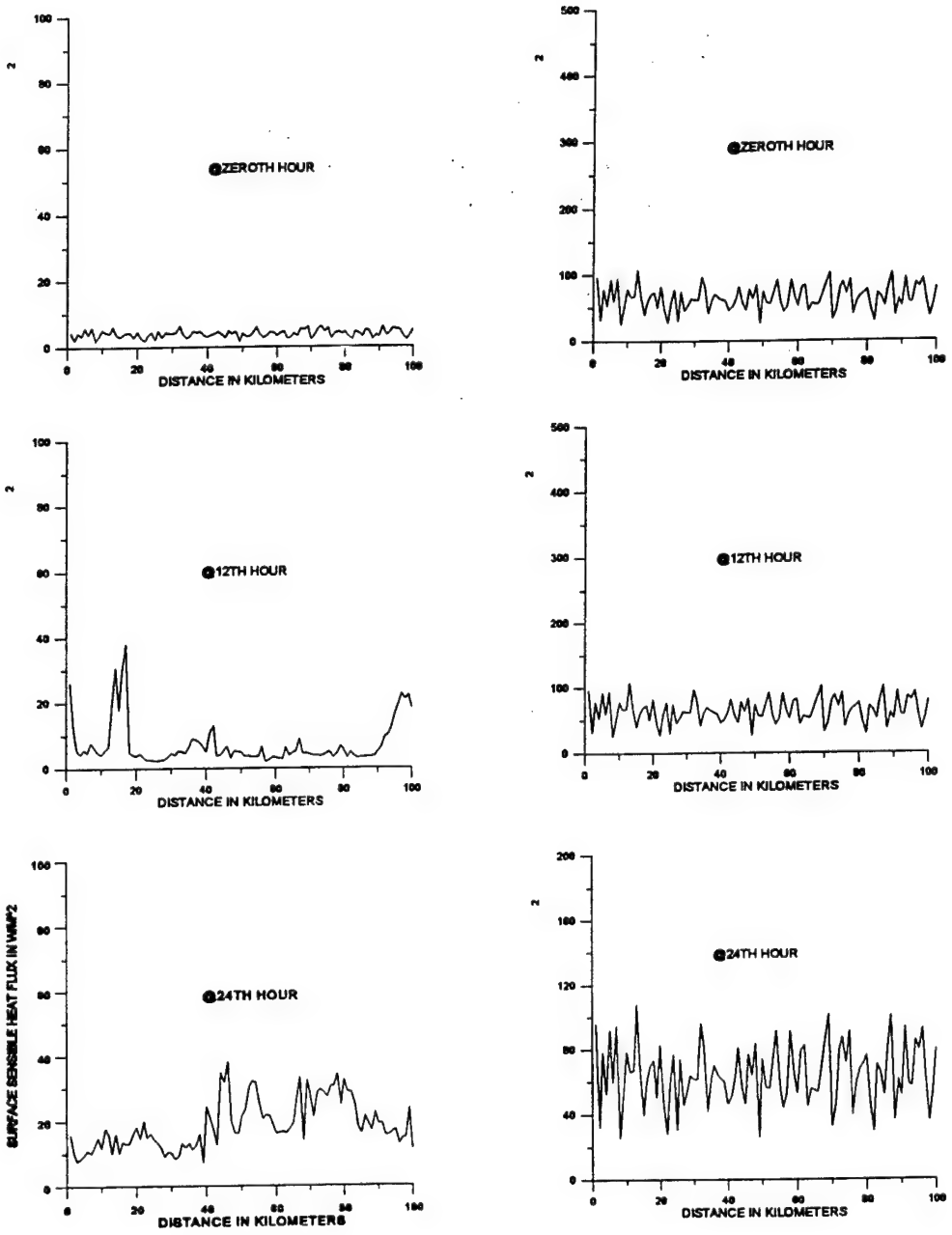

Fig. 13: Sea surface sensible and latent heat flux values

5.2 Experimental Verification of Prediction Results

The hybrid model developed in the program preserves details of turbulence of the second-order-closure model and calculation efficiency of the large-eddy simulation. To establish confidence in prediction accuracy, the cloud profiles predicted in Section 4.3 using the hybrid model shown in figure 14A are compared with the empirical dataset presented in Section 5.1 plotted in figure 14B.

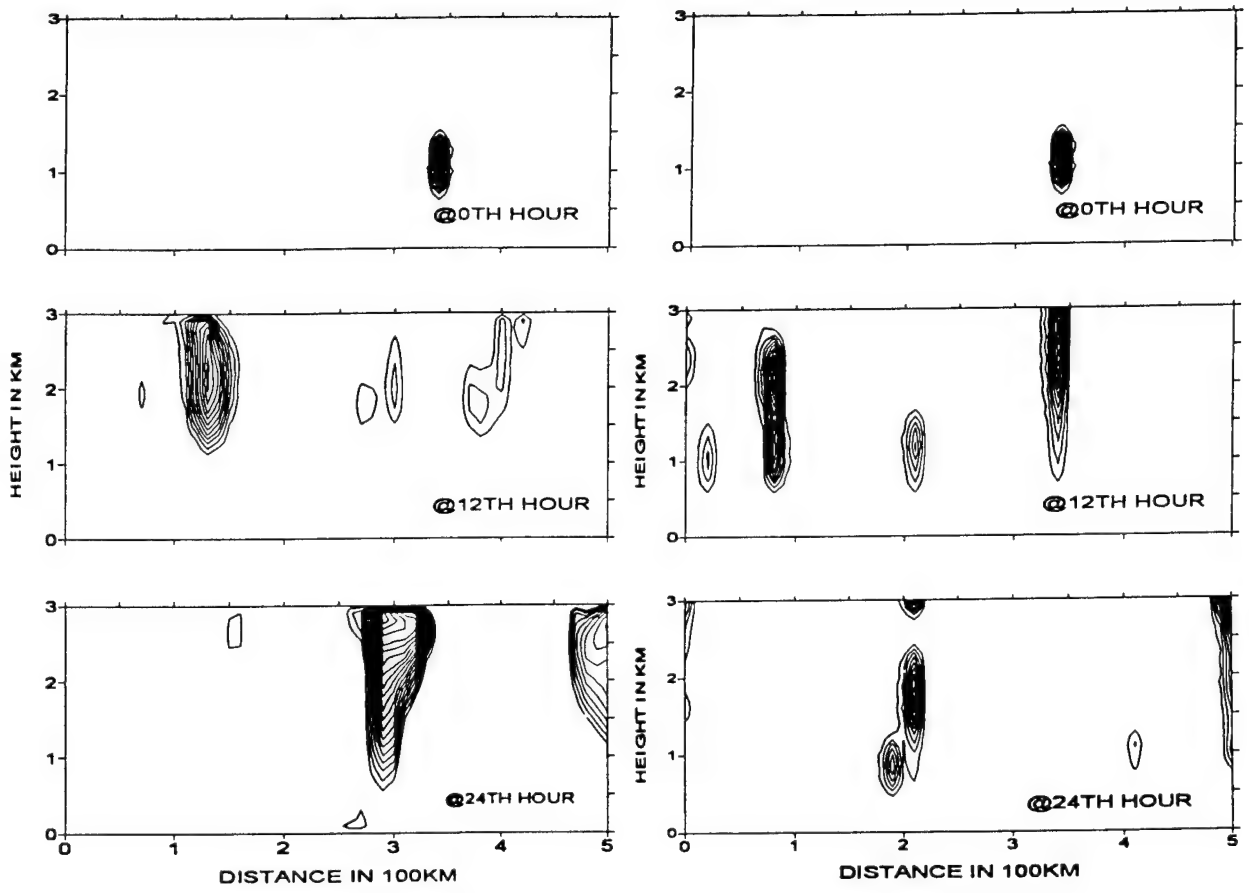

Fig. 14A: Predicted Cloud Profiles

Fig. 14B: Empirical Cloud Profiles

6. CONCLUSION

For goals of research at UDC to identify physical processes that determine the dynamics of marine cloud layers and to quantify roles of turbulence, convection and thermal radiation that play in formation, dissipation and stability of the marine cloud layers, the author and his co-workers at UDC have endeavored to achieve the objectives:

- To advance turbulence models using efficient numerical schemes,
- To make available computer simulation programs for predicting stability of marine cloud layers,
- To retrieve web-site data of marine cloud layers from reliable sources,
- To establish confidence in models through experimental verification, and
- To yield insights into the cloud's physical processes.

For these objectives, two turbulent models, using the second-order-closure and the LES model, respectively, have been formulated. A finite-volume procedure has been developed to solve the resultant equations. In addition, to retain turbulence details of the second-order turbulence and calculation efficiencies of the LES model, a hybrid model has been assembled. It uses a multi-dimensional framework of the LES model but uses a set of unidirectional second-order equations to calculate the turbulent intensity values.

For experimental verification of the hybrid model, theoretical results have been compared with relevant empirical data retrieved from reliable sources. Several data sources such as TOGA-COARE (Tropical Ocean Global Atmosphere – Coupled Ocean Atmosphere Response Experiment), GCE (Goddard Cumulus Ensemble), FIFE (The First ISLCP Field Experiment), GDAAC (Goddard DAAC) and others were evaluated based on the time-interval, grid-size and domain criteria.

According to these criteria, two sources of data T0GA-COARE (experimental) and GCE model (semi-empirical) were examined in detail. Through cooperation with the NASA scientists and a permission of using their CRAY computer, several sets of the GCE data were decoded and transmitted to the author. These data have been used to verify the UDC's model simulation results. Figure 14A shows snapshots of cloud profiles that have been predicted by the hybrid model under the same wind-stream-function, air/sea interface sensible and latent heating fluxes and other boundary-condition values that were provided by the empirical data. Although predictions are not expected to have a complete agreement with the experimental data (as precipitation is not considered in the present theory), a good degree of similarity can be observed between the predicted cloud profiles shown in figure 14A and those empirical cloud profiles shown in figure 14B.

6. REFERENCES

Chi, J, 1996: The effect of turbulent heat and moisture transfer on the dynamics of marine cloud layers, Proc. of the ASME Fluids Engineering Division Summer Meeting, San Francisco. **FED236**, 117-232.

Chi, J., 1994: Heat and Moisture Transfer. Ch.15 of the book titled *The Oceans: Physical-Chemical Dynamics and Human Impact*. Ed.: S.K. Majundar, et al., The Pennsylvania Academy of Science, 237-254.

Chi, J., 1998a: Turbulent mixing processes in the marine atmosphere. CD-ROM Proceedings of Fluids Engineering Division Summer Meeting, Washington, DC. Paper No. **FEDSM98-4809**, 6pp.

Chi, J., 1998b: A large-eddy simulation model for dynamics of the marine cloud layer. CD-ROM Proceedings of Fluids Engineering Division Summer Meeting, Washington DC. Paper No. **FEDSM98-4954**, 6pp.

Lin, X., and R.H. Johnson, 1996: Kinematic and thermodynamic characteristics of the flow over the western Pacific warm pool during TOGA COARE. J. Atmos. Sci., **53**, 2232-2242.

Miller, E.R., and A.C. Riddle, 1994: TOGA COARE integrated sounding system data report - Volume 1A. Available from TOGA-COARE International Project Office, UCAR, P.O. Box 3000, Boulder, CO 80307.

Moeng, C.H., and A. Arakawa, 1980: A numerical study of a marine subtropical stratus cloud layer and its stability. J. Atmos. Sci., **37**, 2661-2576.

Mellor, G.L., and T. Yamada, 1974: A hierarchy of turbulence closure models for planetary boundary layers. J. Atmos. Sci., **31**, 1791-1806.

Nuss, W. A., and D.W. Titley, 1994: Use of multi quadric interpolation for meteorological objective analysis. Mon. Wea. Rev., **22**, 1611-1631.

Patanka, S.V., 1980: *Numerical Heat Transfer and Fluid Flow*. McGraw-Hill, New York, NY, 193pp.

Tao, W.K., and J. Simpson, 1993: Goddard cumulus ensemble model. Part 1: Model description. J. Terr. Atmos. and Ocean Sci., **4**, no.1, 35-72.

Webster, P.J., and R. Lukas, 1992: TOGA COARE: The Coupled Ocean-Atmosphere Response Experiment. Bull. Amer. Meteor., **73**, 1377-1416.

Reprints of a Paper From
Proceedings of the ASME Fluids Engineering Summary Meeting Conference, San Diego, CA,
Vol.236, 227-232, (1996)

APPENDIX A

THE EFFECTS OF TURBULENT HEAT AND MOISTURE TRANSFER ON THE DYNAMICS OF MARINE CLOUD LAYERS

The American Society of Mechanical Engineers

Reprinted From
FED-VOL. 236, Proceedings of the ASME Fluids Engineering Summer Meeting
Conference Chair: H. W. Coleman
Book No. H01072 – 1996

THE EFFECTS OF TURBULENT HEAT AND MOISTURE TRANSFER ON THE DYNAMICS OF MARINE CLOUD LAYERS

Joseph Chi

University of the District of Columbia
Department of Mechanical Engineering
4200 Connecticut Avenue, NW, MB4202
Washington, DC 20008-1174
U. S. A.

Telephone: (202)274-5047
Fax: (202)274-6311
E-mail: 76775-1104@compuserve.com

ABSTRACT

A study has been made to identify physical processes that determine the dynamics of the marine atmosphere and its cloud layers. The effort starts from formulation of the governing equations for conservation of momentum, enthalpy and moisture of atmospheric air. The turbulence transport equations are derived to calculate the Reynolds-stress and turbulence-flux correlations that appear in the conservation equations. The thermal radiation equations are derived to calculate the radiation flux divergence. A virtual dry potential temperature value is introduced to account for the effects of water vapor condensation and cloud formation on the transport of the turbulence quantities. A simulation computer program is developed to calculate dynamic responses of the marine atmosphere and its cloud layers. Results of numerical experiments have led us to a better understanding of the effects of heat and moisture exchange between air and sea, cloud-top radiative cooling, and interactions of atmospheric turbulence and thermal radiation on the dynamics of marine cloud layers.

INTRODUCTION

Advances in turbulence modeling and computational techniques have made it a common practice to study numerically the turbulent-flow problems (Mellor and Yamada, 1974; Moeng and Arakawa, 1980; Moeng and Randall, 1984; Chi, 1991). Several studies of turbulent flows, e.g., using the eddy-viscosity model for a tornado-like vortex (Chi and Jih, 1974), the large-eddy-simulation model for end-wall boundary layers of intense vortices (Chi, 1977), the ϵ-k model for vortex flows over the water surface (Chi, 1987) and the second-order closure model for heat and moisture transfer in marine atmospheres (Chi, 1994), have been reported earlier. In this paper, a study of the simultaneous effects of turbulent heat and moisture transfer, water vapor condensation and thermal radiation on the dynamics of marine cloud layers is presented.

CONSERVATION AND TURBULENCE EQUATIONS

Let U, V and W be the mean velocity components in the east, north and vertical (x,y,z) directions and at the time t, F_R the radiation flux, Θ the mean moist-air potential temperature defined as $[T+(gz+L\Omega_v)/C_p]$, and Ω the mean total moisture mixing ratio of vapor and liquid water (Q_v+Q_l). The lowercase symbols u, v, w, θ and ω represent the turbulent fluctuation quantities corresponding to their respective mean quantities U, V, W, Θ and Ω. In addition, the following definitions will be used: L for the water latent heat of vaporization, C_p the constant pressure specific heat, T the temperature, g the gravitational acceleration, f the Coriolis parameter, Θ_v the virtual dry potential temperature defined as $[T(1+1.609\Omega_v-\Omega)+gz/C_p]$, and ρ the density. Far above a sea surface, the geostrophic balance is assumed. It gives the following relationship between the pressure field and horizontal velocity components U_g and V_g (Holton, 1972):

$$-fV_g = -\frac{1}{\rho}\frac{\partial P}{\partial x} \qquad (1)$$

$$fU_g = -\frac{1}{\rho}\frac{\partial P}{\partial y} \qquad (2)$$

In addition, equilibrium of velocity and temperature between phases is assumed, and a Boussinesq approximation is used. Consequently, the conservation equations for momentum, enthalpy and moisture of atmospheric air can be written as:

$$\frac{\partial U}{\partial t} = f(V-V_g) - \frac{\partial uw}{\partial z} - W\frac{\partial U}{\partial z} \qquad (3)$$

$$\frac{\partial V}{\partial t}=f(U_g-U)-\frac{\partial \overline{vw}}{\partial z}-W\frac{\partial V}{\partial z} \qquad (4)$$

$$\frac{\partial \Theta}{\partial t}=-W\frac{\partial \Theta}{\partial z}-\frac{\partial \overline{w\theta}}{\partial z}-\frac{1}{\rho C_p}\frac{\partial F_R}{\partial z} \qquad (5)$$

$$\frac{\partial \Omega}{\partial t}=-W\frac{\partial \Omega}{\partial z}-\frac{\partial \overline{w\omega}}{\partial z} \qquad (6)$$

The turbulent transport equations (Chi, 1991) derived from the second-order-closure assumption can be used to solve a set of the fifteen turbulent variables $\overline{u^2}$, $\overline{v^2}$, $\overline{w^2}$, $\overline{uv}$, $\overline{uw}$, $\overline{vw}$, $\overline{u\theta}$, $\overline{v\theta}$, $\overline{w\theta}$, $\overline{u\omega}$, $\overline{v\omega}$, $\overline{w\omega}$, $\overline{\theta^2}$, $\overline{\theta\omega}$, and $\overline{\omega^2}$; they include the variables $\overline{wu}$, $\overline{wv}$, $\overline{w\theta}$, and $\overline{w\omega}$ in Eq. (1-4). To allow for water vapor condensation and cloud formation, the buoyancy terms associated with fluctuation of the virtual dry potential temperature, $\overline{u\theta_v}$, $\overline{v\theta_v}$, $\overline{w\theta_v}$, $\overline{\theta\theta_v}$, and $\overline{\omega\theta_v}$ appear in the turbulence transport equations; they may be calculated from the predicted turbulence variables, using the following equations for the clear and cloudy layers, respectively:

$$\overline{\xi\theta_v}=\overline{\xi\theta}+(0.609\phi-1)\frac{L}{C_p}\overline{\xi\omega} \qquad (7)$$

$$\overline{\xi\theta_v}=\frac{1+1.609\phi\gamma}{1+\gamma}\overline{\xi\theta}-\phi\frac{L}{C_p}\overline{\xi\omega} \qquad (8)$$

Here ξ represents any turbulence quantities, u, v, w, etc.; ϕ is equal to C_pT/L; γ is equal to $(L/C_p)\partial\Omega^*/\partial T$; and superscript * represents values at the saturation state.

THERMAL RADIATION EQUATIONS

The radiation calculation requires a large amount of time. Simple emissivity approach using the gray-gas assumption has been used. The theory discussed by Sparrow and Cess (1966) was followed. By applying the boundary conditions of the blackbody radiation at the sea-surface and zero downward radiation at the top of the atmosphere, and letting E be the mixed water-vapor-and-cloud emissivity value, the thermal radiation flux F_R can be calculated by the equation:

$$F_R=\sigma T_o^4 e^{-\frac{3}{2}E_z}+\frac{3}{2}e^{-\frac{3}{2}E_z}\int_0^z \sigma T^4 e^{\frac{3}{2}E}\frac{dE}{dz}dz$$

$$-\frac{3}{2}e^{\frac{3}{2}E_z}\int_z^{\infty}\sigma T^4 e^{-\frac{3}{2}E}\frac{dE}{dz}d \qquad (9)$$

Here, E_z represents the emissivity value E at the height z where the F_R value is being calculated.

NUMERICAL PROCEDURE AND COMPUTER ALGORITHM

The conservation and turbulence transport equations discussed above can be written in the following general form:

$$\frac{\partial \alpha}{\partial t}+U_j\frac{\partial \alpha}{\partial x_j}-\frac{\partial}{\partial x_j}(\gamma\frac{\partial \alpha}{\partial x_j})+\phi=0, \textit{ within domain } \Omega \qquad (10)$$

and their boundary and initial conditions may be written as:

$$\gamma\frac{\partial \alpha}{\partial n}+a\alpha+b=0, \textit{ on boundary } \Gamma \qquad (11)$$

$$\alpha(x,y,z,0)=\alpha_0(x,y,z), \textit{ at initial time zero} \qquad (12)$$

where $\alpha(z,t)$ are mean values of velocity components, enthalpy, moisture and turbulent correlations; $\phi(z,t)$ values are sources/sinks for α; the Four items in Eq. (10) describe the system's inertia, convection, diffusion and source/sink strength, respectively; and values of 'a' and 'b' in Eq. (11) may be specified to enforce the appropriate boundary conditions.

A finite-element procedure (Chi, 1994) is used for the discretization of spatial variables. The flow domain to be simulated is divided into small finite elements. Multiplying both sides of Eq. (10) by a weighing function ω and integrating over the finite element Ω_e, the weighted residual equation set can be derived:

$$\int_{\Omega_e}\omega[\frac{\partial \alpha}{\partial t}+U_j\frac{\partial \alpha}{\partial x_j}-\frac{\partial}{\partial x_j}(\gamma\frac{\partial \alpha}{\partial x_j})+\phi]d\tau=0 \qquad (13)$$

Integrating the second-order term in Eq. (13) by parts and substituting Eq. (11) for normal gradients at the element's boundary result in the following equation:

$$\int_{\Omega_e}[\omega\frac{d\alpha}{dt}+\gamma\frac{\partial \omega}{\partial x_j}\frac{\partial \alpha}{\partial x_j}+U_j\omega\frac{\partial \alpha}{\partial x_j}+\phi]d\tau+\oint_{\Gamma_e}(a\omega\alpha+b\omega)d\sigma=0 \qquad (14)$$

The weighing functions ω and dependent variables $\alpha(x,y,z,t)$ are interpolated in each element Ω_e as follows:

$$\omega_e(z)=\psi_n(z)\Omega_n \qquad (15)$$

$$\alpha_e(z,t)=\psi_n(z)A_n(t) \qquad (16)$$

where ψ_n denotes the interpolation functions at the nth node of each finite element, and A_n and Ω_n are the element nodal values of the variable α and the weighing function ω, respectively.

Substituting Eq. (15) and (16) into Eq. (14) yields the following finite-element equation:

$$C_{mn}\frac{dA_n}{dt}+(K_{mn}+U_{mn}+H_{mn})A_n+L_n=0 \qquad (17)$$

where C_{mn}, K_{mn}, U_{mn} and H_{mn} are the mth-row and nth-column elements of square matrices which describe distributions of the finite element's capacitance, diffusivity, convectiveness and surface flux, respectively, and L_n is the nth element of a load vector for the finite-element source/sink terms.

Assembling the finite-element Eq. (17) over the whole flow field yields a set of ordinary differential equations:

$$[C]\frac{d\{A\}}{dt}+[K+U+H]\{A\}+[L]=0 \qquad (18)$$

Where the vector $\{A\}$ contains all node point variables lying within the flow domain Ω; the matrices [C], [K], [U] and [H] represent global distributions of capacitance, diffusiveness, convection and surface conductance, respectively; and [L] is the global load vector.

The finite-element procedure described above has trans-formed the initial value partial differential conservation and turbulence transport equations into a large-order system of the ordinary differential equation set (18). Solution of (18) may start from a Taylor series expansion of $\{A\}$ about time t:

$$\{A\}_{n+1}=\{A_n\}+\Delta t[\theta\frac{\partial\{A\}_{n+1}}{\partial t}+(1-\theta)\frac{\partial\{A\}_n}{\partial t}] \qquad (19)$$

where θ is an implicit coefficient. Multiplying both sides of Eq. (19) by capacitance matrix [C], Eq. (19) may be re-written as:

$$\{F(A_{n+1})\}=[C][\{A\}_{n+1}-\{A_n\}-(\Delta T)\theta\frac{\partial\{A\}_{n+1}}{\partial t}-(\Delta t)(1-\theta)\frac{\partial\{A\}_n}{\partial t}] \qquad (20)$$

With expressions for time derivatives provided by Eq. (18), Eq. (20) becomes:

$$\{F\}=[C]_{n+1}(\{A\}_{n+1}-\{A\}_n)$$
$$+\Delta t\,\theta([K+U+H]_{n+1}\{A\}_{n+1}+\{L\}_{n+1}$$
$$+\Delta t(1-\theta)([K+U+H]_n\{A\}_n+\{L\}_n) \qquad (21)$$

The equation set (21) may be solved for $\{A\}_{n+1}$ values at time t_{n+1} from the known $\{A\}_n$ values at time t_n by a Newton's iterative process. A computer program has been written to facilitate the process. The resultant computer program can be used to simulate the dynamics of the marine atmosphere and its cloud layers. Presented below are two examples of simulation results.

RESULTS AND DISCUSSION

Firstly, a numerical experiment was made to show responses of a marine atmosphere to variations of the sea surface temperature. Here the geostrophic wind velocity aligned in the x direction is set at a constant value of 10 m/s; the Coriolis parameter f is set at 1.0×10^{-4} s^{-1}; and the sea surface roughness parameter z_o is set at 0.1 m. Initially, the vertical profiles of the potential temperature are chosen to be well-mixed at 290 °K and have a total mixing ratio value corresponding to 100 percent relative humidity at the top of the marine planetary boundary layer (MPBL). Just above the MPBL top at z equal to 1 km, there is an inversion layer 400 m thick, in which temperature increases and mixing ratio decreases at 0.02 °K/m and 8×10^{-6} m^{-1}, respectively. Above the inversion top, the gradient of temperature is -0.005 °K/m and that of the mixing ratio is zero. Subsequently, the sea-surface temperature is allowed to vary. Numerical simulations are made to experiment on the dynamic responses of the marine atmosphere to variations of the sea-surface temperature.

Figure 1 shows a hypothetical cyclic sinusoidal temperature variation of the sea surface. Calculations were allowed to proceed for five days with the sea-surface temperature repeating cyclically every twenty four hours. Shown in Fig. 2 through 4 are predicted cyclic variations over a twenty-four-hour period of the mean wind-velocity and air-potential-temperature distributions at different time. Predicted responses of turbulent energy, horizontal components of the Reynolds stress and vertical component of the enthalpy flux are shown in Fig. 5 through 8.

Many interesting characteristics of the marine planetary boundary layer (MPBL) can be observed in these figures. It can be seen in Fig. 1 that the sea-surface temperature was set to rise during the hours of six to eighteen and fall during the hours of eighteen to six. As the sea-surface temperature falls (rises), stability of the boundary layer increases (decreases). The trends can be seen in Fig. 2 and 3 by decreasing in the marine surface boundary layer thickness during the hours of eighteen to six and increasing in the marine surface boundary layer thickness during the hours of eighteen to six. In particular, instability of the marine thermal boundary layer can be observed in the vicinity of the eighteenth hour when the sea-surface temperature is at its maximum. It can be observed also in Fig. 5 where contours of the turbulent energy values at different height and time are shown. Instability of the MPBL in the vicinity of the eighteenth hour can be seen also in this figure. Although it can be observed in this figure, the maximum thickness of the MPBL in the experiment does not occur at the exact time of the maximum sea-surface temperature at the eighteenth hour (but at approximately the 21st hour) because of delay in the responses. Similarly, the effects of stability on distribution of the horizontal components of the Reynolds stress and the vertical component of the heat flux can be seen in Fig. 6 to 8. Again, instabilities of the MPBL can be seen in these figures by observing the maximum stress and flux values and increasing in the MPBL thickness in the vicinity of the eighteenth hour.

For the second case of numerical experiments, its initial conditions at the zeroth hour are obtained from the eighteenth-hour results of the first-case experiments presented above. In this case, the sea-surface temperature is changed at the zeroth hour to 298°K, and it is maintained, thereafter, at this constant value. The sea-surface-air moisture mixing ratio is maintained at the corresponding saturated

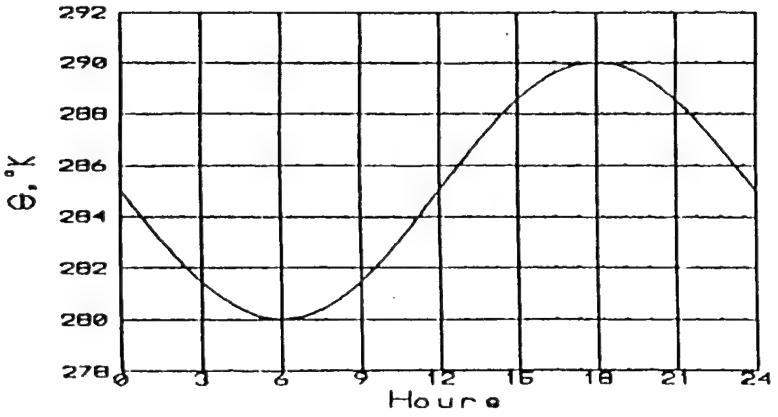

Fig. 1 Sea surface temperature variation, Θ °K

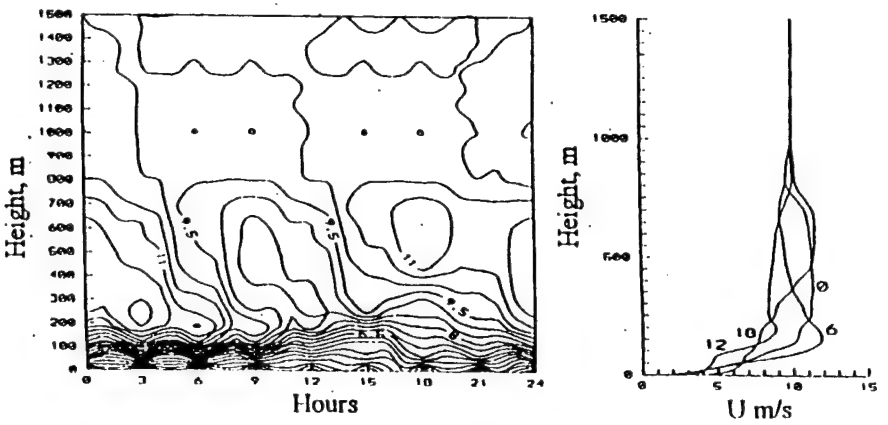

Fig. 2 X-component mean wind velocity, U m/s

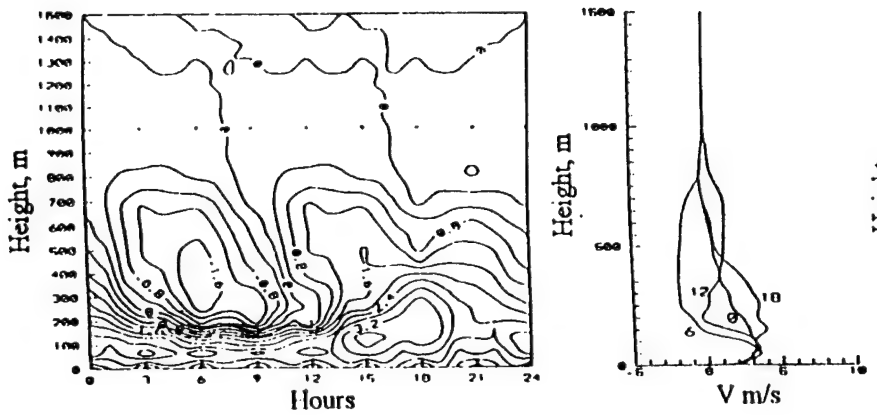

Fig. 3 Y-Component mean wind velocity, V m/s

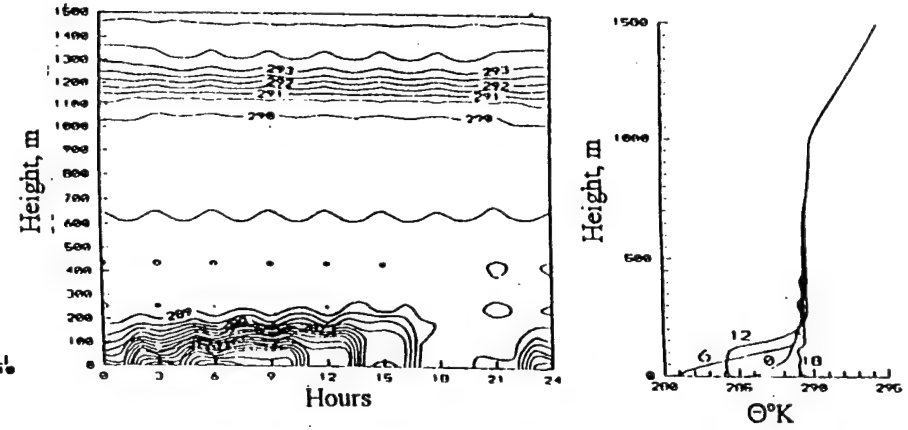

Fig. 4 Mean air potential temperature, Θ °K

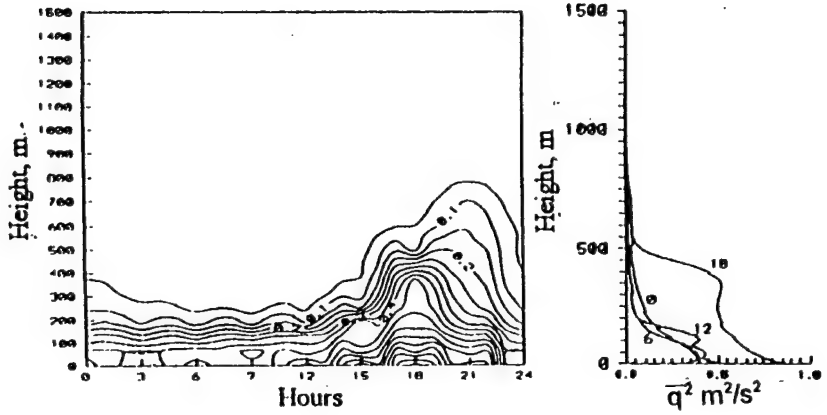

Fig. 5 Turbulent energy, $\overline{q^2}$ m²/s²

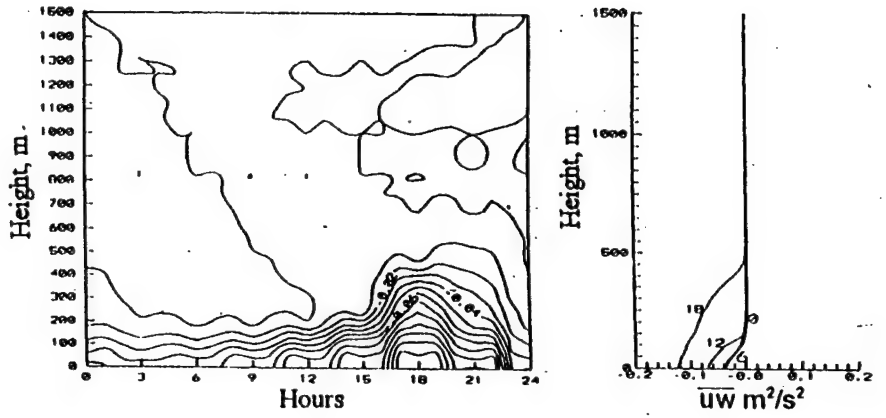

Fig. 6 X-component Reynolds strees, $\overline{uw}$ m²/s²

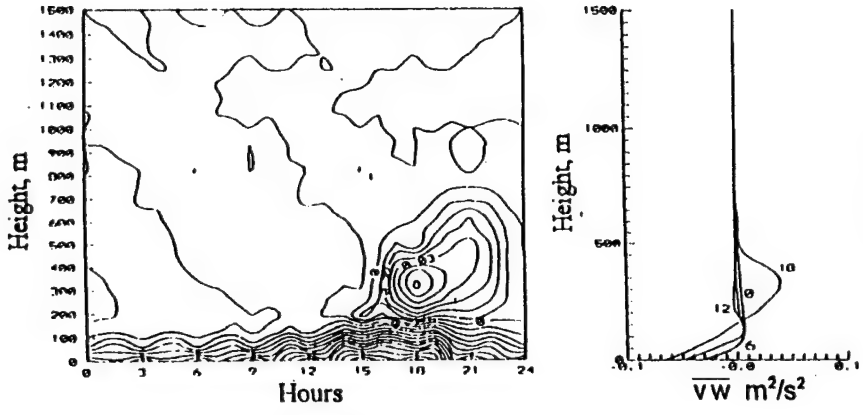

Fig. 7 Y-Component Reynolds stress, $\overline{vw}$ m²/s²

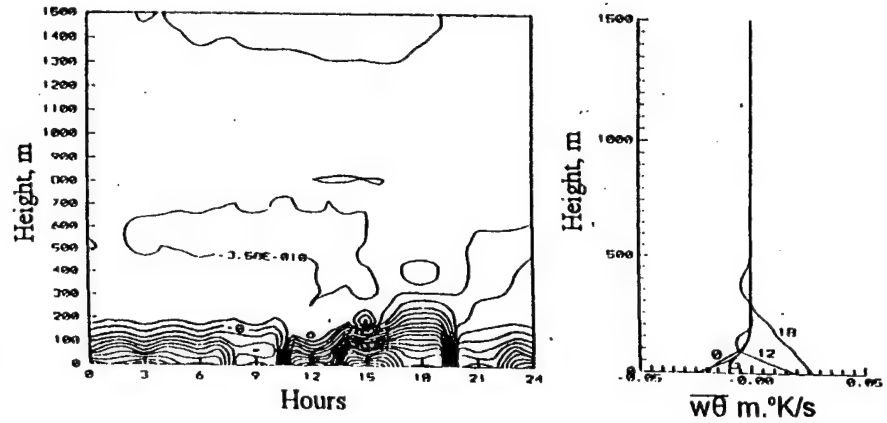

Fig. 8 Turbulent enthalpy stress, $\overline{w\theta}$ m.°K/s

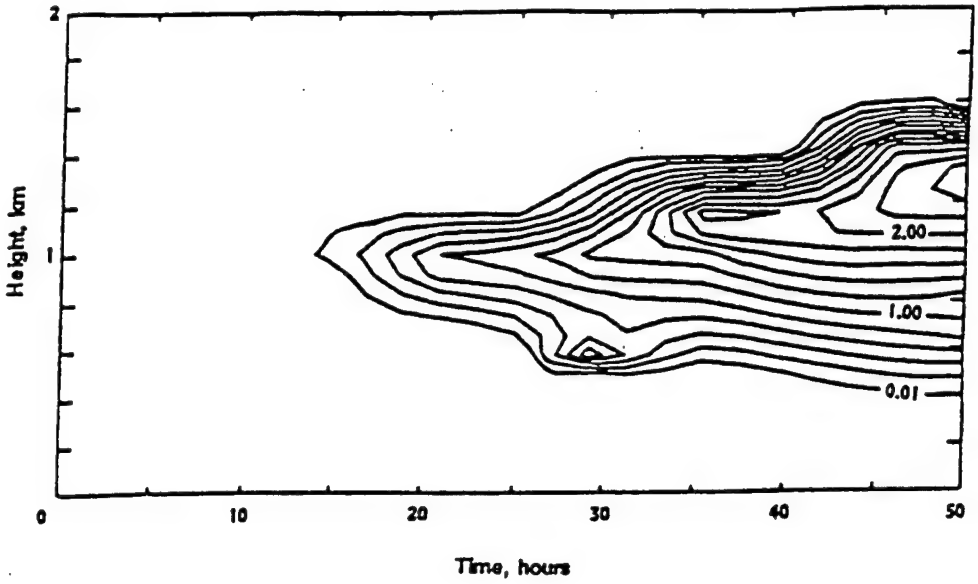

Fig. 9 Contours of predicted cloud intensity of the liquid-water mixing ratio in g/kg

state. Plotted in Fig. (9) are contours of the predicted cloud intensity of the liquid-water mixing ratio values in g/kg. It can be seen in this figure that the cloud starts to form at the 14th hour. Its depth grows firstly downward because of the upward transport of the water vapor from the sea surface and the upward drop in the static temperature of the air. From the 25th hour onwards, because of the cloud-top radiative cooling, the depth of the cloud increases at the top. Also, it can be seen in this figure that the steady state of the cloud layer was reached at about the 48th hour.

CONCLUSION

In conclusion a numerical study of turbulence in marine atmospheres has been made. Results of predictions have led us to a better understanding of the effects of air/sea heat and moisture exchange, cloud-top radiative cooling, and interactions of atmospheric turbulence and thermal radiation on the dynamics of marine cloud layers.

ACKNOWLEDGMENT

This work has been partially supported by the Office of Naval Research; the author wishes to express his appreciation for its support.

REFERENCES

Chi, J., 1977, "Numerical analysis of turbulent end-wall boundary layers of intense vortices," *J. Fluid Mech.*, 82, 209-222.

Chi, J., 1987, "Heat, moisture and momentum transfer in turbulent vortex flows over the water surface," Proc. ASME/ JSME Thermal Eng. Joint *Conf.*, 627-633.

Chi, J., 1991, "Prediction of Reynolds stress and heat flux in stratified shear layers, " *Proc. SES Annual Technical Meeting*, 28, 8pp.

Chi, J., 1994, "Heat and Moisture Transfer," Ch.15 of the book entitled *The Oceans: Physical-Chemical Dynamics and Human Impact.* Ed. S.K. Majumdar, E.W. Miller, G. S. Forbes, R.F. Schmatz and A.A. Panah. The Pennsylvania Academy of Science. 237-254.

Chi, J., and J. Jih, 1974, "Numerical modeling of the three-dimensional flows in the ground boundary layer of a maintained axisymmetrical vortex," *TELLUS*, 26, 444-455. Holton, J.R., 1972, *An Introduction to Dynamic Meteorology*, Academic Press, New York, NY, 28-32.

Mellor, G.L., and T. Yamada, 1974, "A hierarchy of turbulence closure models for planetary boundary layer," *J. Atmos. Sci.*, 31, 1791-1806.

Moeng, C. H., and A. Arakawa, 1980, "A numerical study of a marine subtropical stratus cloud layer and its stability," J. Atmos. Sci., 37, 2661-2576.

Moeng, C. H., and D. A. Randall, 1984, "Problems in simulations of the stratocumulus-topped boundary layer with a third-order closure model," J. Atmos. Sci., 42, 1588-1600.

Sparrow, E. M., and R. D. Cess, 1966, *Radiation Heat Transsfer*, Brooks/Cole Publishing Co.,Belmont, CA, 224-238.

Reprints of a Paper From
1998 ASME Fluids Engineering Division Summer Meeting, June 21-25, 1998, Washington, DC.
CD-ROM Proceedings Paper No. Fedsm98-4809, 6pp.

APPENDIX B

TURBULENT MIXING PROCESSES IN THE MARINE ATMOSPHERE

Proceedings of FEDSM'98
1998 ASME Fluids Engineering Division Summer Meeting
June 21-25, 1998, Washington, DC

Paper No. FEDSM98-4809

TURBULENT MIXING PROCESSES IN THE MARINE ATMOSPHERE

Joseph Chi
Department of Mechanical Engineering
University of the District of Columbia
Washington, DC 20008-1174
U.S.A.

Phone: (202)274-5047
Fax: (202)274-6311
E-mail: jchi@compuserve.com

ABSTRACT

Goals of our atmospheric research at UDC are to identify physical processes that determine the dynamics of the cloud layers and to quantify the roles of turbulence, convection and thermal radiation that play in formation, dissipation and stability of the cloud layers. Our immediate objectives are to advance theoretical models, use efficient numerical schemes and develop computer programs to simulate the marine cloud layers. Comparison of computer results with published field observations will yield insights into the cloud-layers' physical processes. While a companion paper FEDSM98-4954 develops a large-eddy turbulent model to simulate stability of the marine cloud layers, this paper describes a second-order closure turbulent model to simulate turbulent mixing of the moist atmospheric air in general and the marine atmospheres in particular.

INTRODUCTION

Turbulent mixing of heat, moisture and momentum plays a dominant role in atmospheric processes that are of interests to scientists of different disciplines: physicists, meteorologists, and environmentalists. Advances in turbulent modeling will lead to better understanding of climatic phenonmena[1,2,8] - cloud stability, tornado motion, and severe-storm formation - and environmental qualities[9,10,13] - air pollution, acid deposition and global warming. Consequently, improvements can be made in climatic prediction and environmental control.

Much of our understanding of mixing processes in atmospheres has come from careful observation and sound theoretical modeling. While it is yet impossible to have a generalized turbulence theory for universal phenomena, semi-empirical models with different degrees of complexity have been developed with confidence in simulating numerous practical phenomena: the mixing-length theory has been used to model turbulent boundary layers on flat plates,[11] the second-order diffusion model has been used for simulating the planetary boundary layers,[6] and large-eddy models have been used to study the meso-scale turbulence in atmospheres.[12] This author[3] has used the eddy-viscosity model to simulate a tornado-like vortex, the large-eddy-turbulence model for end-wall boundary layers of intense vortices, the ϵ-k model for vortex flow over the water surface, and the second-order closure model for the marine cloud layer. It is intended in this study to present a hybrid treatment for the atmospheric turbulence that uses a second-order closure turbulent diffusion model for simulating atmospheric mixing layers and a large-eddy turbulent model for simulating meso-scale entrainment in the marine atmosphere. Presented in this paper is a second-order diffusion model for simulating moisture mixing in the marine atmosphere; a large-eddy model for simulating the cloud-layer entrainment will be presented in a companion paper.[5]

NOMENCLATURE

C_p	=	specific heat
A, B, C, D, E, & F	=	values in turbulent flux equation second-order closure equations' empirical constants
f	=	geostrophic Coriolis coefficient
F_R	=	thermal radiation flux
g	=	gravitational acceleration
L	=	water-vapor latent heat of vaporization
q	=	square-root value of squared mean of the turbulent fluctuating velocity
t	=	time
T	=	static temperature of atmospheric air
(u,v,w)	=	turbulent fluctuating velocities in (x,y,z) directions

(U,V,W) =mean wind velocity components in (x,y,z) directions
(Ug,Vg) =geostrophic wind components in (x,y) directions
(x,y,z) =east-, north- and vertical-direction coordinates
α =a generalized variable in a numerical scheme
β = buoyant coefficient
θ = turbulent fluctuating value of Θ
θ_v = turbulent fluctuating value of Θ_v
Θ = mean potential temperature = $T+(gz+L\Omega_v)/C_p$
Θ_v = mean virtual potential temperature
= $T(1+1.609\Omega_v-\Omega)+gz/C_p$
κ = Prandtl mixing length constant
λ = turbulent length scale
ω = turbulent fluctuating value of Ω
Ω = mean total moisture ratio
Ω_l = mean liquid moisture ratio
Ω_v = mean vapor moisture ratio
Overlined values
= turbulent-flux values
Other symbols in numerical procedures
= those defined in the text

CONSERVATION AND TURBULENCE EQUATIONS

When these assumptions are made: (1) at far above a sea surface, the geostrophic balance is maintained, (2) velocity, temperature of vapor and liquid moisture are in equilibrium, and (3) Boussinesq approximation is used, the conservation equations for momentum, enthalpy and total moisture of atmospheric air can be written as:

$$\frac{\partial U}{\partial t}=f(V-V_g)-\frac{\partial \overline{uw}}{\partial z}-W\frac{\partial U}{\partial z} \quad (1)$$

$$\frac{\partial V}{\partial t}=f(U_g-U)-\frac{\partial \overline{vw}}{\partial z}-W\frac{\partial V}{\partial z} \quad (2)$$

$$\frac{\partial \Theta}{\partial t}=-W\frac{\partial \Theta}{\partial z}-\frac{\partial \overline{w\theta}}{\partial z}-\frac{1}{\rho C_p}\frac{\partial F_R}{\partial z} \quad (3)$$

$$\frac{\partial \Omega}{\partial t}=-W\frac{\partial \Omega}{\partial z}-\frac{\partial \overline{w\omega}}{\partial z} \quad (4)$$

In above equations, values for overlined turbulent -flux values can be calculated by the turbulent transport equations using the assumptions of Mellor and Yamada's second-order closure model:[7]

$$\frac{\partial \overline{u^2}}{\partial t}=\frac{\partial}{\partial z}(Aq\lambda\frac{\partial \overline{u^2}}{\partial z})-2\overline{uw}\frac{\partial U}{\partial z}-B\frac{q}{\lambda}(\overline{u^2}-\frac{q^2}{3})-D\frac{q^3}{3\lambda} \quad (5)$$

$$\frac{\partial \overline{v^2}}{\partial t}=\frac{\partial}{\partial z}(Aq\lambda\frac{\partial \overline{v^2}}{\partial z})-2\overline{vw}\frac{\partial V}{\partial z}-B\frac{q}{\lambda}(\overline{v^2}-\frac{q^2}{3})-D\frac{q^3}{3\lambda} \quad (6)$$

$$\frac{\partial \overline{w^2}}{\partial t}=\frac{\partial}{\partial z}(3Aq\lambda\frac{\partial \overline{w^2}}{\partial z})+2\beta\overline{w\theta}_v-B\frac{q}{\lambda}(\overline{w^2}-\frac{q^2}{3})-D\frac{q^3}{3\lambda} \quad (7)$$

$$\frac{\partial \overline{uw}}{\partial t}=\frac{\partial}{\partial z}(2Aq\lambda\frac{\partial \overline{uw}}{\partial z})+\beta g\overline{u\theta}_v-(\overline{w^2}-C\overline{q^2})\frac{\partial U}{\partial z}-B\frac{q}{\lambda}\overline{uw} \quad (8)$$

$$\frac{\partial \overline{vw}}{\partial t}=\frac{\partial}{\partial z}(2Aq\lambda\frac{\partial \overline{vw}}{\partial z})+\beta g\overline{v\theta}_v-(\overline{w^2}-C\overline{q^2})\frac{\partial V}{\partial z}-B\frac{q}{\lambda}\overline{vw} \quad (9)$$

$$\frac{\partial \overline{u\theta}}{\partial t}=\frac{\partial}{\partial z}(Aq\lambda\frac{\partial \overline{u\theta}}{\partial z})-\overline{uw}\frac{\partial \Theta}{\partial z}-\overline{w\theta}\frac{\partial U}{\partial z}-E\frac{q}{\lambda}\overline{u\theta} \quad (10)$$

$$\frac{\partial \overline{v\theta}}{\partial t}=\frac{\partial}{\partial z}(Aq\lambda\frac{\partial \overline{v\theta}}{\partial z})-\overline{vw}\frac{\partial \Theta}{\partial z}-\overline{w\theta}\frac{\partial V}{\partial z}-E\frac{q}{\lambda}\overline{v\theta} \quad (11)$$

$$\frac{\partial \overline{w\theta}}{\partial t}=\frac{\partial}{\partial z}(2Aq\lambda\frac{\partial \overline{w\theta}}{\partial z})-\overline{w^2}\frac{\partial \Theta}{\partial z}+\beta g\overline{\theta\theta}_v-E\frac{q}{\lambda}\overline{w\theta} \quad (12)$$

$$\frac{\partial \overline{\theta^2}}{\partial t}=\frac{\partial}{\partial z}(Aq\lambda\frac{\partial \overline{\theta^2}}{\partial z})-2\overline{w\theta}\frac{\partial \Theta}{\partial z}-F\frac{q}{\lambda}\overline{\theta^2} \quad (13)$$

$$\frac{\partial \overline{u\omega}}{\partial t}=\frac{\partial}{\partial z}(Aq\lambda\frac{\partial \overline{u\omega}}{\partial z})-\overline{uw}\frac{\partial \Omega}{\partial z}-\overline{w\omega}\frac{\partial U}{\partial z}-E\frac{q}{\lambda}\overline{u\omega} \quad (14)$$

$$\frac{\partial \overline{v\omega}}{\partial t}=\frac{\partial}{\partial z}(Aq\lambda\frac{\partial \overline{v\omega}}{\partial z})-\overline{vw}\frac{\partial \Omega}{\partial z}-\overline{w\omega}\frac{\partial V}{\partial z}-E\frac{q}{\lambda}\overline{v\omega} \quad (15)$$

$$\frac{\partial \overline{w\omega}}{\partial t}=\frac{\partial}{\partial z}(2Aq\lambda\frac{\partial \overline{w\omega}}{\partial z})-\overline{w^2}\frac{\partial \Omega}{\partial z}+\beta g\overline{\omega\theta}_v-E\frac{q}{\lambda}\overline{w\omega} \quad (16)$$

$$\frac{\partial \overline{\omega^2}}{\partial t}=\frac{\partial}{\partial z}(Aq\lambda\frac{\partial \overline{\omega^2}}{\partial z})-2\overline{w\omega}\frac{\partial \Omega}{\partial z}-F\frac{q}{\lambda}\overline{\omega^2} \quad (17)$$

$$\frac{\partial \overline{\theta\omega}}{\partial t}=\frac{\partial}{\partial z}(Aq\lambda\frac{\partial \overline{\theta\omega}}{\partial z})-\overline{w\omega}\frac{\partial \Theta}{\partial z}-\overline{w\theta}\frac{\partial \Omega}{\partial z}-F\frac{q}{\lambda}\overline{\theta\omega} \quad (18)$$

In above equations, λ is a characteristic length scale that is equal to the value of the Blackadar's or the diffusion-length scale - λ_B or λ_D - whichever is the smallest.

In equations 5 through 18, the time-derivative terms on the left-hand side model the transient variation of turbulence correlations. The second-order derivative terms on the right-hand side model turbulent diffusion. While the production of turbulence due to buoyancy is modeled by terms with buoyant coefficient β, the production of turbulence due to friction is modeled by products of second-order correlations and gradients of mean variables. Terms with coefficients B, C, E and F represent the turbulent redistribution. Turbulent dissipation is modeled by terms with coefficient D. Coefficients κ, A, B, C, D, E and F have been determined semi-empirically,[3] having the values equal to 0.35, 0.21, 0.46, 0.053,

0.132, 0.44, and 0.23, respectively.

NUMERICAL PROCEDURE AND COMPUTER ALGORITHM

The conservation and turbulence transport equations 1 to 18 described above can be written in the following general form:

$$\frac{\partial\alpha}{\partial t}+W\frac{\partial\alpha}{\partial z}-\frac{\partial}{\partial z}(\gamma\frac{\partial\alpha}{\partial z})+\phi=0, \quad \textit{Within domain} \qquad (19)$$

The boundary and initial conditions may be written as:

$$\gamma\frac{\partial\alpha}{\partial n}+a\alpha+b=0, \quad \textit{On boundary } \Gamma \qquad (20)$$

$$\alpha(z,0)=\alpha_0(z), \quad \textit{At initial time zero} \qquad (21)$$

In above equations, $\alpha(z,t)$ values are mean values of velocity components, enthalpy, moisture and turbulent correlations; $\phi(z,t)$ values are sources/sinks for α. The Four items in equation 19 describe the system's inertia, convection, diffusion and source/sink strength, respectively. 'a' and 'b' values in equation 20 are used to define the appropriate boundary conditions.

A finite-element procedure[4] was used for descritization of spatial variables. The flow domain to be simulated was divided into small finite elements. Multiplying both sides of equation 19 by a weighing factor and integrating over the finite element, a weighted residue equation set can be derived. Then, substituting into the residue equation a set of appropriate interpolation functions for the weighing factor and the element's variables resulted the following finite-element equation set:

$$C_{mn}\frac{dA_n}{dt}+(K_{mn}+U_{mn}+H_{mn})A_n+L_n=0 \qquad (22)$$

Where C_{mn}, K_{mn}, U_{mn} and H_{mn} are the mth-row and nth-column elements of square matrices which describe distributions of the finite element's capacitance, diffusivity, convectiveness and surface flux, respectively, and L_n is the nth element of a load vector for the finite-element source/sink terms. Finally, assembling the finite-element equation 22 over the whole flow field yielded a set of ordinary differential equations:

$$[C]\frac{d\{A\}}{dt}+[K+U+H]\{A\}+[L]=0 \qquad (23)$$

Where the vector $\{A\}$ contains node-points variables lying within the flow domain Ω, [L] is the global load vector, and the matrices [C], [K], [U] and [H] represent global distributions of capacitance, diffusiveness, convection and surface conductance, respectively.

The finite-element procedure described above has transformed the initial boundary value partial differential equations 1 through 18 into a large-order system of the ordinary differential equation set 23. Solution of 23 may start from a Taylor series expansion of $\{A\}$ about time t_n:

$$\{A\}_{n+1}=\{A_n\}+\Delta t[\theta\frac{\partial\{A\}_{n+1}}{\partial t}+(1-\theta)\frac{\partial\{A\}_n}{\partial t}] \qquad (24)$$

where θ is an implicit coefficient. Multiplying both sides of equation 24 by capacitance [C] and using expressions for time derivatives provided by equation 23, equation 24 becomes:

$$\begin{aligned}\{F\}=&[C]_{n+1}(\{A\}_{n+1}-\{A\}_n)\\&+\Delta t\theta([K+U+H]_{n+1}\{A\}_{n+1}+\{L\}_{n+1})\\&+\Delta t(1-\theta)([K+U+H]_n\{A\}_n+\{L\}_n)\end{aligned} \qquad (25)$$

The equation set 25 may be solved for the vector $\{A\}_{n+1}$ at time t_{n+1} from the known $\{A\}_n$ values at time t_n by a Newton's iterative process, and a computer program has been written to facilitate the process. The resultant computer program can be used to simulate mixing processes in the marine atmosphere. Presented below is an example of computer-simulation results.

RESULTS AND DISCUSSION

The above-described computer program has been used to predict transient exchange of moisture in the sea/air interface, mixing of moisture in the marine atmosphere, and formation of the cloud layer. Graphs plotted in figure 1 were reported in a previous paper;[4] they were used as initial conditions for this study.

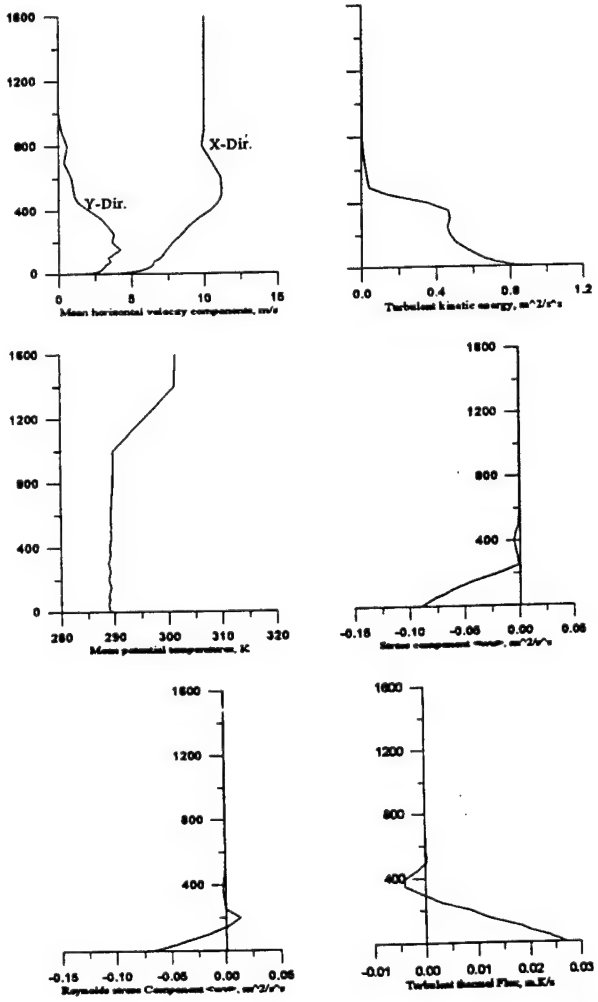

Fig.1: Initial Velocity-Components and Potential-Temperature Values

The initial conditions shown in figure 1 were obtained on the assumptions that the geostrophic wind in the x-direction was at 10m/s, and Coriolis parameter f is equal to 1.0×10^{-4} s^{-1}, the potential temperature was chosen to be well-mixed at 290K, and the total moisture mixing ratio corresponding to 100 percent relative humidity at top of the marine planetary boundary layer (MPBL). Just above the MPBL top at height equal to 1 km, there was an inversion layer of 400-m thick, in which temperature was increasing at 0.2 K/m and moisture mixing ratio was decreasing at 0.008 g/kg.m, respectively. The sea-surface temperature was allowed to vary diurnally within the range of 280 to 290F. Conditions shown in figure 1 were for the instance when the sea surface was at 290 K.

For the simulation run using initial conditions shown in figure 1, it was assumed that the sea surface temperature was raised abruptly to and then maintained at 298 K, and the air total moisture ratio at the sea surface was maintained at the saturation state. After a simulation run over a period of forty hours, a large body of data was generated. Plotted in figures 2 are predicted contours of temporal mean physical-property values of air in the marine atmosphere; plotted in figures 3 are predicted contours of Reynolds-stress and turbulent-flux values in the marine atmosphere. Many interesting characteristics of mixing in the simulation domain can be observed in these contours. Firstly, rapid interaction at the air/sea interface can be observed during the initial period of zero to 600 minutes. It is followed by a calmer development of the marine planetary boundary layer for about 600 minutes. Then, during the next 600 minutes transfer of enthalpy and moisture continues, as can be observed from the predicted contours of the turbulent thermal- and moisture-flux values shown in figures 3C and 3D. Also, can be observed in Fig. 2D is the formation of cloud starting at the 200th minute, rapid deepening of the cloud layer during the second interval of 200 to 1200 minutes, and slower growth of the cloud layer during the period of 1200 to 1800 minutes. Finally, a steady state is established at around the 2400th minute.

Plotted in figure 4 are the predicted steady-state conditions at the end of the simulation period of the 40th hour. These graphs shown in figure 4 can be compared with those in figure 1 for the initial conditions. Changes that have been made during these forty hours can be observed. Firstly, warm and moist air at the sea surface has resulted in an unstable mixing layer. It can be observed by comparison of the mean horizontal velocity components plotted in figures 1A and 4A of the thickening of the unstable boundary layer in figure 4A due to the intensed turbulent exchange. It can also be observed in figure 4H of the increased turbulent kinetic energy in comparison with the corresponding turbulent-energy values plotted in figure 1. In addition, variations of profiles for the mean wind velocity, mean potential temperature, mean total-moisture ratio, mean liquid-moisture ratios, Reynolds-stress, turbulent thermal flux, turbulent moisture flux and turbulent kinetic energy can be observed in figure 4.

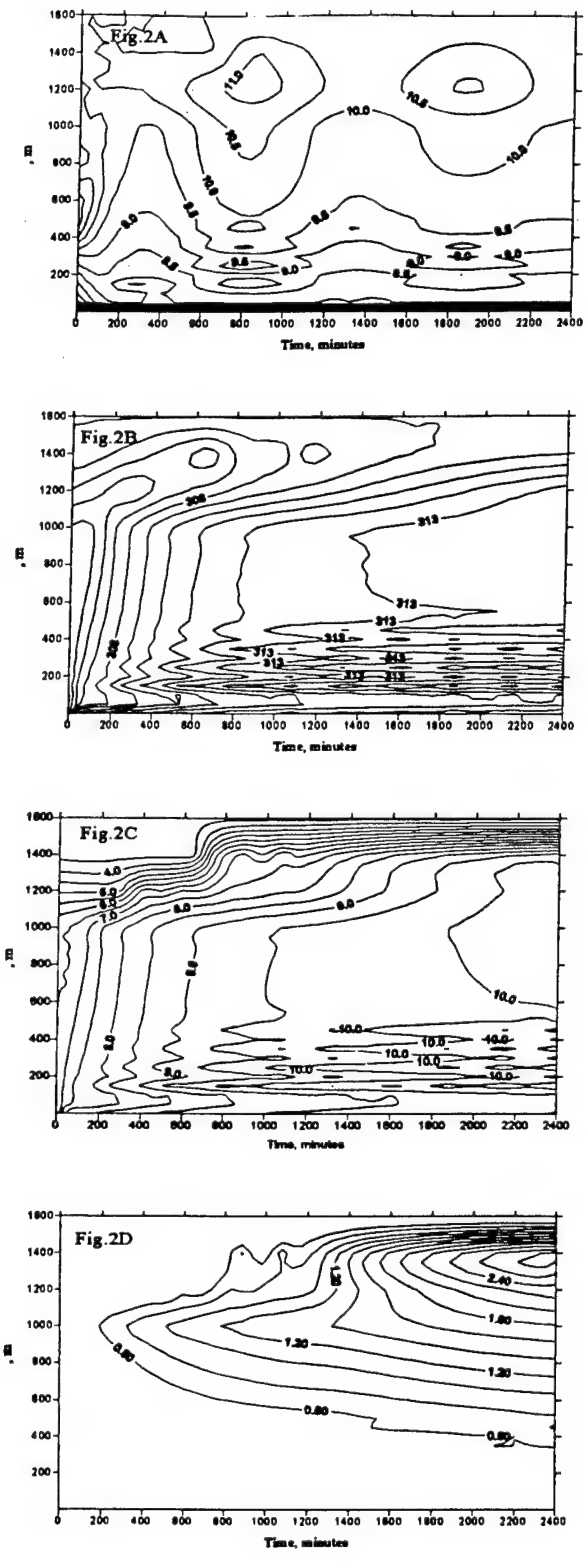

Fig. 2: Predicted Contours of Mean Atmospheric Quantities
2A - Mean Wind Velocity, m/s
2B - Mean Potential Temperature, K
2C - Mean total moisture mixing ratio, g/kg
2D - Mean liquid moisture mixing ratio, g/kg

CONCLUSION

In conclusion, a numerical study of turbulent mixing of moist air in the marine atmosphere has been made. Results of predictions have led us to a better understanding of the turbulent mixing process in the atmosphere. However, complexity of the turbulent model has limited our study to a one-dimensional model. Physics learned in this study has led us to the development of a multidimensional large-

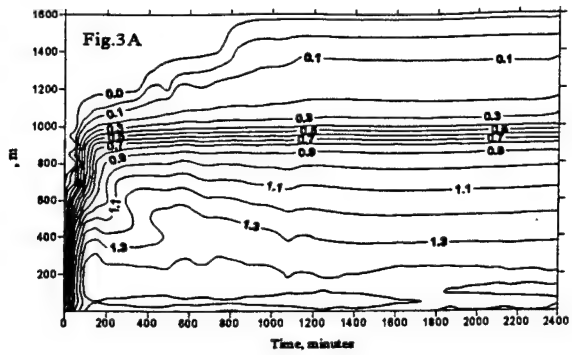

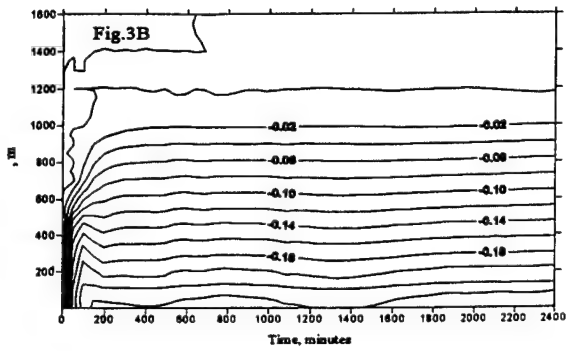

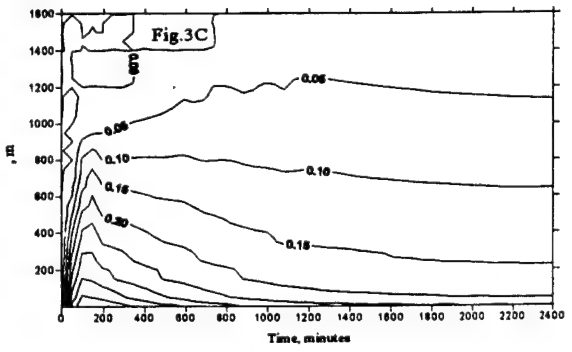

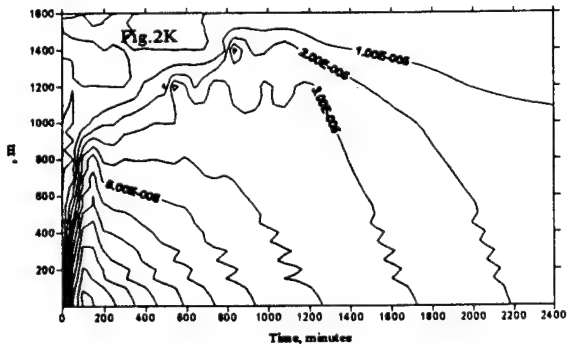

Fig. 3: Predicted Contours of Turbulent Fluxes
3A - Turbulent kinetic energy, m^2/s^2
3B - Principal Reynolds stress, m^2/s^2
3C - Turbulent thermal flux, m.K/s
3D - Turbulent moisture flux, m.kg/kg.s3

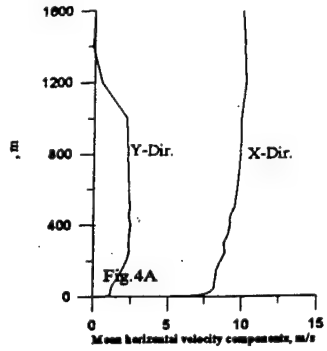

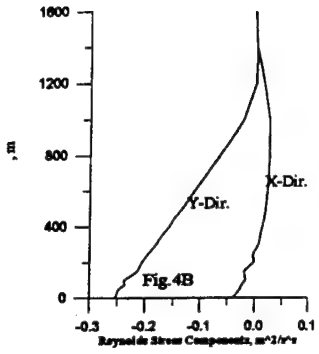

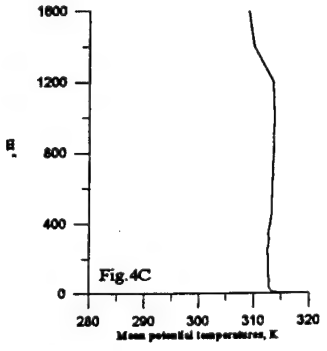

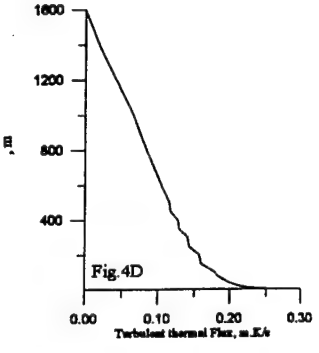

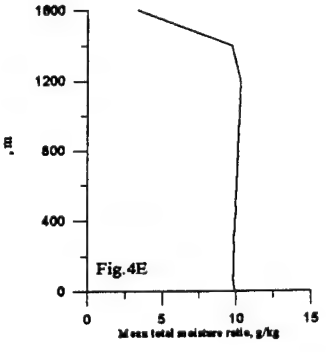

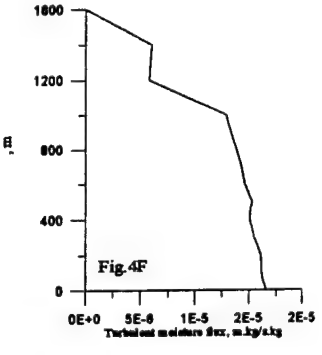

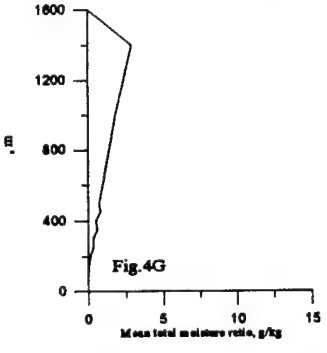

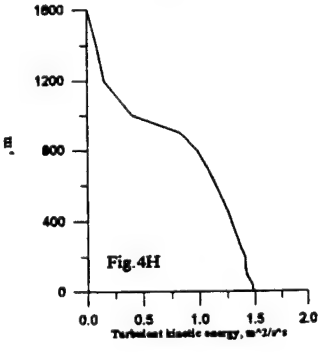

Fig. 4: Predicted Mean Quantities and Turbulent Fluxes
4A - Mean velocity; 4B - Reynolds stress;
4C - Potential temperature; 4D - Thermal flux;
4E - Total moisture ratio; 4F - Moisture flux;
4G - Liquid moisture ratio; 4H - Turbulent energy.

eddy turbulent model for investigating stability of the marine cloud layer.[5]

ACKNOWLEDGMENTS

This work has been supported by the Office of Naval Research; the author wishes to express his appreciation for its support.

REFERENCES

[1]Chi, J., 1977: Numerical modeling of the three-dimensional flows in the ground boundary layer of a maintained axisymmetrical vortex, *TELLUS*, **26**, 444-455.

[2]Chi, J., 1987: Heat, moisture and momentum transfer in turbulent vortex flows over the water surface. *Proc. ASME/JSME Thermal Engineering Joint Conf.*, 627-633.

[3]Chi, J., 1994: Heat and Moisture Transfer. Ch.15 of the book titled *The Oceans: Physical-Chemical Dynamics and Human Impact.* Ed.: S.K. Majundar, et al., The Pennsylvania Academy of Science, 237-254.

[4]Chi, J., 1996: The effects of turbulent heat and moisture transfer on the dynamics of marine cloud layers. *Proc. ASME Fluids Engineering Summer Meeting*, **236**, 227-232.

[5]Chi, J., 1998: A large eddy simulation model for dynamics of the the marine cloud layers, *ASME Fluids Engineering Division Annual Meeting*, Paper No. FEDSM98-4954, 6pp.

[6]Lewellen, W.S., M.E. Teske, and U.P. Sheng, 1980: Micrometeorological applications of a secon-order closure model of turbulent transport, *Turbulent Shear Flows*, **2**, 366-378.

[7]Mellor, G.L., and T. Yamada, 1974: A hierarchy of turbulence closure models for planetary boundary layer. *J. Atmos. Sci.*, **31**, 1791-1806.

[8]Moeng, C.H., and A. Arakawa, 1980: A numerical study of a marine subtropical stratus cloud layer and its stability, *J. Atmos. Sci.*, **37**, 2661-2576.

[9]Sempere, R., and K. Kawamura, K., 1994: Comparative distributions of dicarboxylic acids and related polar compounds in snow, rain and aerosols from urban atmosphere. *Atmospheric Environment*, **28**, 449-459.

[10]Sirois, A., 1993: Temporal variation of sulphate and nitrate concetration in precipitation in eastern North America: 1997-1990. *Atmospheric Environment.* **27**, 945-963.

[11]Spalding, D.B., and J. (S.W.) Chi, 1964: The drag of a compressible turbulent boundary layer on a smooth flat plate with and without heat transfer. ***J.Fluid Mech.***, **18**, 114-143.

[12]Sykes, R.I., and D.S. Henn, 1989: Large-eddy simulation of turbulent sheared convection, *J. Atmos. Sci.*, **46**, 1106-1118.

[13]Thurston, G.D., Gorczynski, J.E.,Jr.,and James, H, 1994: The nature and origins of acid summer haze air pollution in metropolitan toronto, Ontario, *Environmental Research*, **65**, 254-270.

Reprints of a Paper From
1998 ASME Fluids Engineering Division Summer Meeting, June 21-25, 1998, Washington, DC.
CD-ROM Proceedings Paper No. Fedsm98-4954, 6pp.

APPENDIX C

A LARGE-EDDY SIMULATION MODEL FOR DYNAMICS OF THE MARINE CLOUD LAYERS

Proceedings of FEDSM'98
1998 ASME Fluids Engineering Division Summer Meeting
June 21-25, 1998, Washington, DC

Paper No. FEDSM98-4954

A LARGE-EDDY SIMULATION MODEL FOR DYNAMICS OF THE MARINE CLOUD LAYERS

Joseph Chi
Department of Mechanical Engineering
University of the District of Columbia
Washington, DC 20008-1174
U.S.A.

Phone: (202)274-5047
Fax: (202)274-6311
E-mail: jchi@compuserve.com

ABSTRACT

Goals of our atmospheric research at University of the District of Columbia (UDC) are to identify physical processes that determine the dynamics of the cloud layers and to quantify the roles of turbulence, convection and thermal radiation that play in formation, dissipation and stability of the cloud layers. Our immediate objectives are to advance theoretical models, use efficient numerical schemes and develop computer programs to simulate the marine cloud layers. Comparison of computer results with published field observations will yield insights into the cloud-layers' physical processes. While a companion paper FEDSM98-4809 develops a second-order closure model for simulating turbulent mixing of the moist marine atmosphere, this paper deals with a large-eddy turbulent model for simulating stability of the marine cloud layers.

INTRODUCTION

Much of our understanding of turbulent processes has come from careful observation and sound theoretical modeling. While it is yet impossible to have a generalized turbulence theory for universal phenomena, semi-empirical models with different degrees of complexity have been developed with confidence in simulating numerous practical phenomena: the mixing-length theory has been used to model turbulent boundary layers on flat plates.[11] the second-order diffusion model has been used for simulating the planetary boundary layers,[7,8,9] and large-eddy models have been used to study the meso-scale turbulence in atmospheres.[10,12] This author has used the eddy-viscosity model to simulate a tornado-like vortex,[1] the large-eddy-turbulence model for end-wall boundary layers of intense vortices,[2] the ϵ-k model for vortex flow over the water surface,[3,4] and the second-order closure model for the marine cloud layers.[5,6] This study of the author uses a hybrid treatment for the atmospheric turbulence that employs a second-order closure turbulent diffusion model for simulating atmospheric mixing layers and a large-eddy turbulent model for simulating convective entrainment at the cloud top. The stratus cloud plays an important role in climatic dynamics; it has stimulated extensive research. Second- and higher-order turbulent models have succeeded in advancing theoretical understanding of the marine cloud layers. Complexity of those models often makes long-term simulation of the cloud layer over an extensive period prohibitively expensive. A hybrid model using second-order bottom-up mixing and large-eddy top-down convection will improve in computational efficiency.

NOMENCLATURE

Symbols:

a,b	=	coefficients in boundary-layer or numerical equations
C_p	=	specific heat
D	=	diffusion parameter
E	=	turbulent kinetic energy
F	=	convection flux parameter
g	=	gravitational acceleration
K	=	eddy coefficient values
L	=	water-vapor latent heat of vaporization
P	=	pressure
t	=	time
T	=	resolved mean static temperature of atmospheric air

(U,V,W) = resolved mean wind velocities in (x,y,z) directions
(u,v,w) = turbulent fluctuating velocities in (x,y,z) directions
(x,y,z) = east-, north- and vertical-direction coordinates
α = a generalized variable in a numerical scheme
β = buoyant coefficient
Γ = diffusivity value in the generalized differential equation
γ = diffusivity value in the generalized boundary condition
δ = a length scale defined by equation 18
($\Delta x,\Delta y,\Delta z$) = node points' distance in (x,y,z) directions
ϵ = a turbulent energy dissipation rate
η = a moisture parameter defined as $(L/C_p)\partial\Omega^*/\partial T$
Θ = resolved mean potential temperature = $T+(gz+L\Omega_v)/C_p$
Θ_v = resolved mean virtual potential temperature
= $T(1+1.609\Omega_v-\Omega)+gz/C_p$
Ω = resolved mean total moisture mixing ratio
= $\Omega_v+\Omega_l$
Ω^* = saturation moisture mixing ratio value at air temperature
Λ = a defined domain under simulation
λ = turbulence-length scales
ξ = a moisture parameter defined as C_pT/L
Π = a defined domain boundary
ρ = air density
σ = turbulent Prandtl number
ϕ = source terms in generalized differential equations

Suffices:

app = for intermediate approximate value in an iterative process
e = for turbulent kinetic energy
ℓ = for liquid water
m = for momentum
o = for a reference state
(P,E,W,B,T) = for a variable node point in a domain element's center and its neighboring node pointes at the east, west, top and bottom
(p,e,w,b,t) = for a velocity node point on an edge of the domain element and its neighboring velocity node pointes at the east, west, top and bottom
v = for water vapor
θ = for enthalpy
ω = for moisture

CONSERVATION AND TURBULENCE EQUATIONS

When these assumptions are made: (1) the Coriolis force is negligible, (2) velocity and temperature of vapor and liquid moisture are in equilibrium, and (3) Boussinesq approximations are used, the conservation equations for momentum, enthalpy and total moisture of atmospheric air can be written as:

$$\frac{\partial U}{\partial t}=2\frac{\partial}{\partial x}(K_m\frac{\partial U}{\partial x})+\frac{\partial}{\partial z}[K_m(\frac{\partial U}{\partial z}+\frac{\partial W}{\partial x})] -U\frac{\partial U}{\partial x}-W\frac{\partial U}{\partial z}-\frac{1}{\rho_o}\frac{\partial P}{\partial z} \quad (1)$$

$$\frac{\partial W}{\partial t}=\frac{\partial}{\partial x}[K_m(\frac{\partial U}{\partial z}+\frac{\partial W}{\partial x})]+2\frac{\partial}{\partial z}(K_m\frac{\partial W}{\partial Z})+\beta g(\Theta-\Theta_o) -U\frac{\partial W}{\partial x}-W\frac{\partial W}{\partial z}-\frac{1}{\rho_o}\frac{\partial P}{\partial z} \quad (2)$$

$$\frac{\partial \Theta}{\partial t}=\frac{\partial}{\partial x}(K_\theta\frac{\partial \Theta}{\partial x})+\frac{\partial}{\partial z}(K_\theta\frac{\partial \Theta}{\partial z})-U\frac{\partial \Theta}{\partial x}-W\frac{\partial \Theta}{\partial z} \quad (3)$$

$$\frac{\partial \Omega}{\partial t}=\frac{\partial}{\partial x}(K_\omega\frac{\partial \Omega}{\partial x})+\frac{\partial}{\partial z}(K_\omega\frac{\partial \Omega}{\partial z})-U\frac{\partial \Omega}{\partial x}-W\frac{\partial \Omega}{\partial z} \quad (4)$$

$$\frac{\partial E}{\partial t}=-[U\frac{\partial E}{\partial x}+W\frac{\partial E}{\partial z}]+\frac{\partial}{\partial x}[K_E\frac{\partial E}{\partial x}]+\frac{\partial}{\partial z}[K_E\frac{\partial E}{\partial z}]+[-\frac{\beta}{\theta_o}\frac{\partial \theta}{\partial z} +2K_m(\frac{\partial U}{\partial x})^2+K_m(\frac{\partial U}{\partial z}+\frac{\partial W}{\partial x})^2+2K_m(\frac{\partial W}{\partial z})^2]-\epsilon \quad (7)$$

$$\frac{\partial U}{\partial x}+\frac{\partial W}{\partial z}=0 \quad (6)$$

In above equations, the buoyancy terms associated with the virtual dry potential temperature have been defined as follows:

$$\Theta_v=T(1+1.609\Omega_v-\Omega)+\frac{gz}{C_p} \quad (7)$$

$$\frac{\partial \Theta_v}{\partial z}=\frac{\partial \Theta}{\partial z}+(0.609\xi-1)\frac{L}{C_p}\frac{\partial \Omega}{\partial z} \quad (8)$$

For Clear Air Layers

$$\frac{\partial \Theta_v}{\partial z}=\frac{1+1.609\xi\eta}{1+\eta}\frac{\partial \Theta}{\partial z}-\xi\frac{L}{C_p}\frac{\partial \Omega}{\partial z} \quad (9)$$

For Cloudy Air Layers

The rate of dissipation within the grid volume and the subgrid eddy coefficient may be parameterized through

$$\epsilon=0.19E^{3/2}/\lambda \quad (10)$$

$$K_m=0.58E^{1/2}\lambda \quad (11)$$

$$K_\theta=\frac{K_m}{\sigma_\theta}(1+\frac{2\lambda}{\lambda_S}) \quad (12)$$

$$K_\omega=\frac{K_m}{\sigma_\omega}(1+\frac{2\lambda}{\lambda_S}) \quad (13)$$

$$K_{ea}=\frac{K_m}{\sigma_e} \quad (14)$$

where λ is a minimum of the Blackadar's length λ_B, diffusion length λ_D, resolvable length scale λ_S:

$$\lambda_B=\frac{0.35z\delta}{\delta+3.5z} \quad (15)$$

$$\lambda_D=0.75(\frac{e\theta\partial z}{g\partial\theta_v})^{1/2} \quad (16)$$

$$\lambda_S=(\Delta x\Delta x\Delta z)^{1/3} \quad (17)$$

$$\delta=\frac{\int_0^\infty E^{1/2}zdz}{\int_0^\infty E^{1/2}dz} \quad (18)$$

And the terms σ_θ, σ_ω, and λ, which are the turbulent Prandtl numbers of enthalpy, moisture and turbulent-energy transports, are equal to 0.75, 0.75 and 1, respectively.

NUMERICAL PROCEDURE AND COMPUTER ALGORITHM

The conservation and turbulence transport equations 1 to 5 described above can be written in the following general form:

$$\frac{\partial\alpha}{\partial t}+U\frac{\partial\alpha}{\partial x}+W\frac{\partial\alpha}{\partial z}=-\frac{\partial}{\partial x}(\Gamma\frac{\partial\alpha}{\partial x})-\frac{\partial}{\partial z}(\Gamma\frac{\partial\alpha}{\partial z})+\Phi \quad (19)$$
within Domain Λ

The boundary and initial conditions may be written as:

$$\gamma\frac{\partial\alpha}{\partial n}+a\alpha+b=0, \quad \textit{On boundary } \Pi \quad (20)$$

$$\alpha(x,z,t=0)=\alpha_0(x,z), \quad \textit{At initial time zero} \quad (21)$$

In above equations, $\alpha(x,z,t)$ values are variable values of velocity components U and W, potential temperature Θ, moisture mixing ratio Ω, and turbulent kinetic energy 'E'; $\phi(x,z,t)$ values are the source/sink terms for α. Items in equation 19 describe the variables' time derivative, convection, diffusion and source/sink strength, respectively. 'a' and 'b' values in equation 20 are used to define the appropriate boundary conditions.

A finite-volume difference scheme[13] was used for descritization of variables. The flow domain to be simulated was divided into small rectangular elements; shown in figure 1 are examples of several such elements. It can be seen in figure 1 that variable values at node points of the elements are strategically located. The node point for velocity value is located in the middle of the rectangular edge and the node point for other variables is located in the center of the rectangular box.

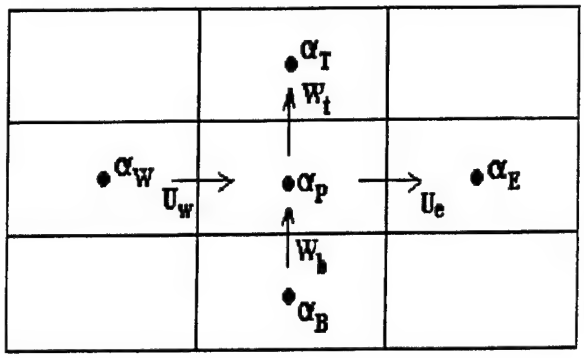

Fig. 1: An Element with Neighboring Variables Shown

Using the velocity values and values of α shown in the figure and employing an upwind logic, the conservation law may be applied to obtain an expression for the value of α at the node point P in terms of the α-values at its neighboring node points:

$$a_P\alpha_P=a_E\alpha_E+a_W\alpha_W+a_T\alpha_T+a_B\alpha_B+b \quad (22)$$

where coefficient values 'a' and 'b' may be expressed in terms of the diffusion and flux parameters defined as follows:

$$a_E=\frac{K_e\Delta z}{\Delta x_e}+Max[-(U_e\Delta z),0] \quad (23)$$

$$a_W=\frac{K_w\Delta z}{\Delta x_w}+Max[(U_w\Delta z),0] \quad (25)$$

$$a_T=\frac{K_t\Delta x}{\Delta z_t}+Max[-(U_t\Delta x),0] \quad (26)$$

$$a_B=\frac{K_b\Delta x}{\Delta z_b}+Max[(U_b\Delta x),0] \quad (27)$$

$$a_P=a_E+a_W+a_T+a_B+\frac{\Delta x\Delta z}{\Delta t} \quad (28)$$

$$b=\phi_P \Delta x \Delta z \tag{29}$$

In addition, in solving U and W values using equation 22, the initial pressure values will have to be the estimated values; consequently, the equation 22 will yield initially approximate U_{app} and W_{app} values. Improved U and W values may be calculated from their approximate values using equations:

$$U_e = U_{e,app} + \frac{\Delta z}{a_P \rho_o}(P_P - P_E) \tag{30}$$

$$U_w = U_{w,app} + \frac{\Delta z}{a_P \rho_o}(P_w - P_P) \tag{31}$$

$$W_t = W_{t,app} + \frac{\Delta x}{a_P \rho_o}(P_P - P_T) \tag{32}$$

$$W_b = W_{b,app} + \frac{\Delta x}{a_P \rho_o}(P_b - P_P) \tag{33}$$

Substituting U and W values in equations 30-33 into the continuity equation 6 yields a set of linear equations for pressure values at the solution domain's node points; they may be used to solve for improved pressure values. So the process may be repeated to iterate alternatively for improved values of velocity, pressure and other variables at the node points.

Using the linear equations discussed above for variable values U, W, Θ, Ω, E and P at node points, a computer program has been written to simulate dynamics of the marine cloud layers.

RESULTS AND DISCUSSION

The above-described computer program may be used to study stability of the marine cloud layers. Graphs plotted in figure 2 show characteristics of a horizontally uniform cloud layer predicted by a one-dimensional turbulent model.[6] It may be noted that solutions for this set of graphs were obtained by using the main stream wind velocity U equal to 10 m/s. To investigate effects of cloud-top-warm-air entrainment on stability of the cloud layer shown in figure 2, a stream function shown in figure 3 will be superimposed to the main flow. In generating the stream function shown in figure 3, the top-down entrainment was assumed to be at a maximum rate of 6 cm/s is at the top-left corner and the rate was reduced sinusoidally to zero at the top-right corner. In addition, it is assumed that potential temperature of the entrained air is at five degrees centigrade higher than that of the cloud at the top.

Using the initial conditions and entrainment rates described above, the present large-eddy simulation computer program has been run. Shown in figure 4 are contours of the initial steady-state potential temperature values, total moisture mixing ratio values and liquid moisture Mixing values, respectively. Predicted dynamic responses of the cloud layer's liquid moisture content to the warm-air entrainment at the top are shown in figure 5. From snapshots shown in this figure of the cloud contours at different times (i.e., at half, one, five and ten hours from the start of the simulation run), dissipation of the cloud layer can be observed.

CONCLUSION

In a companion paper,[6] a second-order closure model was developed to simulate sea-to-air heat and moisture transfer and to observe theoretically the growth of the marine cloud layers. Results of predictions have led us to a better understanding of the turbulent mixing process in the atmosphere. However, complexity of the high-order closure model had limited our study to the mixing layer problems in one dimension. Physics learned in that study has led us to the development of a multidimensional large-eddy turbulent model presented in this paper. The extended theory has enabled us to investigate multidimensional effects of convective entrainment at the cloud top on the dynamics of the marine cloud layers. These quantitative results have provided us at UDC with theoretical tools to identify processes observed physically in the marine cloud layers.

ACKNOWLEDGMENTS

This work has been supported by the Office of Naval Research; the author wishes to express his appreciation for its support.

REFERENCES

[1]Chi, J., 1977: Numerical modeling of the three-dimensional flows in the ground boundary layer of a maintained axisymmetrical vortex, *TELLUS*, **26**, 444-455.

[2]Chi, J., 1977: Numerical analysis of turbulent end-wall boundary layers of intense vortices. *J. Fluid Mech.*, **82**, 209-222.

[3]Chi, J., 1987: Heat, moisture and momentum transfer in turbulent vortex flows over the water surface. *Proc. ASME/JSME Thermal Engineering Joint Conf.*, 627-633.

[4]Chi, J., 1994: Heat and Moisture Transfer. Ch.15 of the book titled *The Oceans: Physical-Chemical Dynamics and Human Impact.* Ed.: S.K. Majundar, et al., The Pennsylvania Academy of Science, 237-254.

[5]Chi, J., 1996: The effects of turbulent heat and moisture transfer on the dynamics of marine cloud layers. *Proc. ASME Fluids Engineering Summer Meeting*, **236**, 227-232.

[6]Chi, J.,1998: Turbulent mixing processes in the marine atmosphere, *ASME Fluids Engineering Division Annual Meeting,* Paper No. FEDSM98-4809, 6pp.

[7]Lewellen, W.S., M.E. Teske, and U.P. Sheng, 1980: Micrometeorological applications of a second-order closure model of turbulent transport, *Turbulent Shear Flows*, **2**, 366-378.

[8]Mellor, G.L., and T. Yamada, 1974: A hierarchy of turbulence closure models for a planetary boundary layer. *J. Atmos. Sci.*, **31**, 1791-1806.

[9]Moeng, C.H., and A. Arakawa, 1980: A numerical study of a marine subtropical stratus cloud layer and its stability, *J.Atmos. Sci.*, **37**, 2661-2576.

[10]Moeng, C.H., 1986: Large-eddy simulation of a stratus-topped boundary layer. *J. Atmos. Sci.*, **43**, 2886-2900.

[11]Spalding, D.B., and J. (S.W.) Chi, 1964: The drag of a compressible turbulent boundary layer on a smooth flat plate with and without heat transfer. ***J.Fluid Mech.***, **18**, 114-143.

[12]Sykes, R.I., and D.S. Henn, 1989: Large-eddy simulation of turbulent sheared convection, *J. Atmos. Sci.*, **46**, 1106-1118.

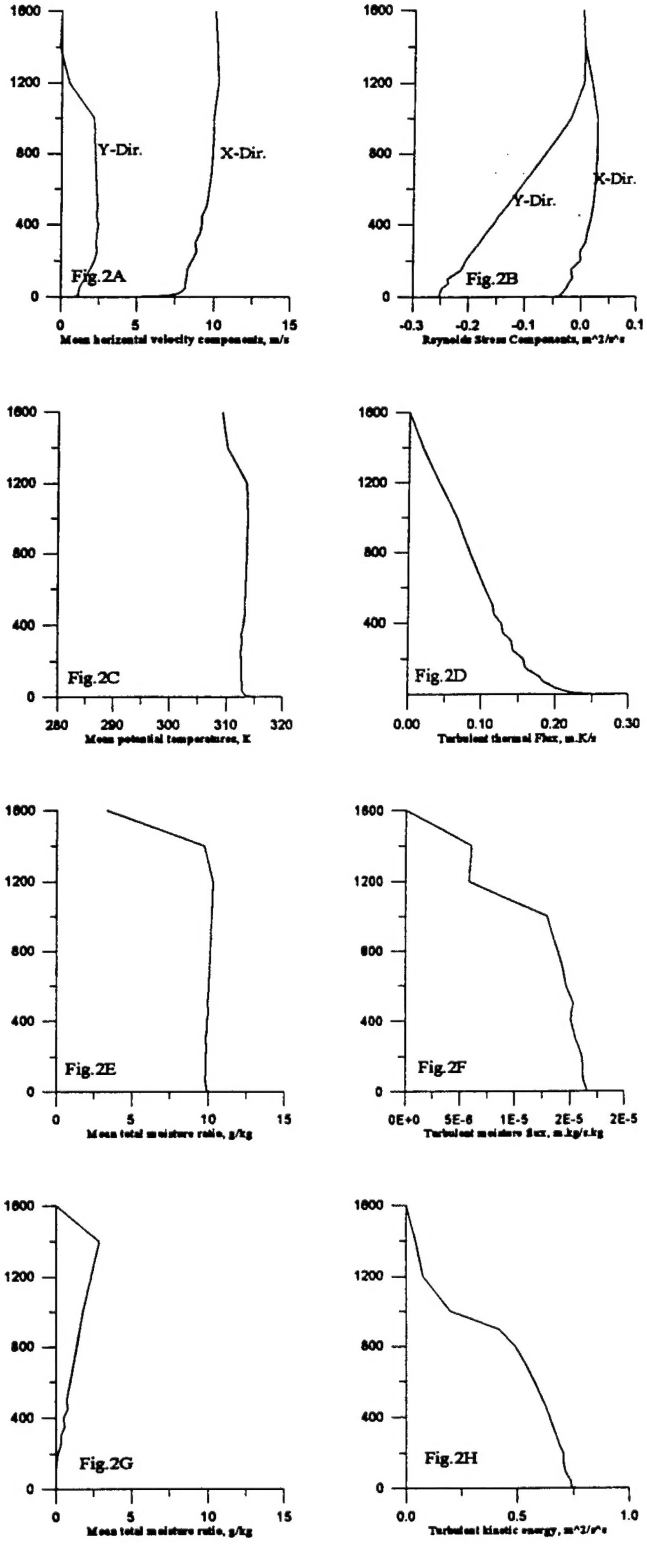

Fig. 2: Characteristics of an Initial Steady-State Cloud Layer
2A - Mean velocity; 2B - Reynolds stress;
2C - Potential temperature; 2D - Thermal flux;
2E - Total moisture ratio; 2E - Moisture flux;
2G - Liquid moistureratio; 2H - Turbulent K.E.

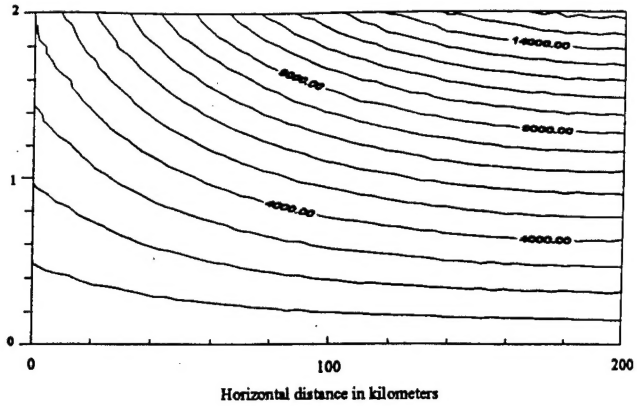

Fig. 3: Contours of Superposed Stream Functions with Entrainment at the Top

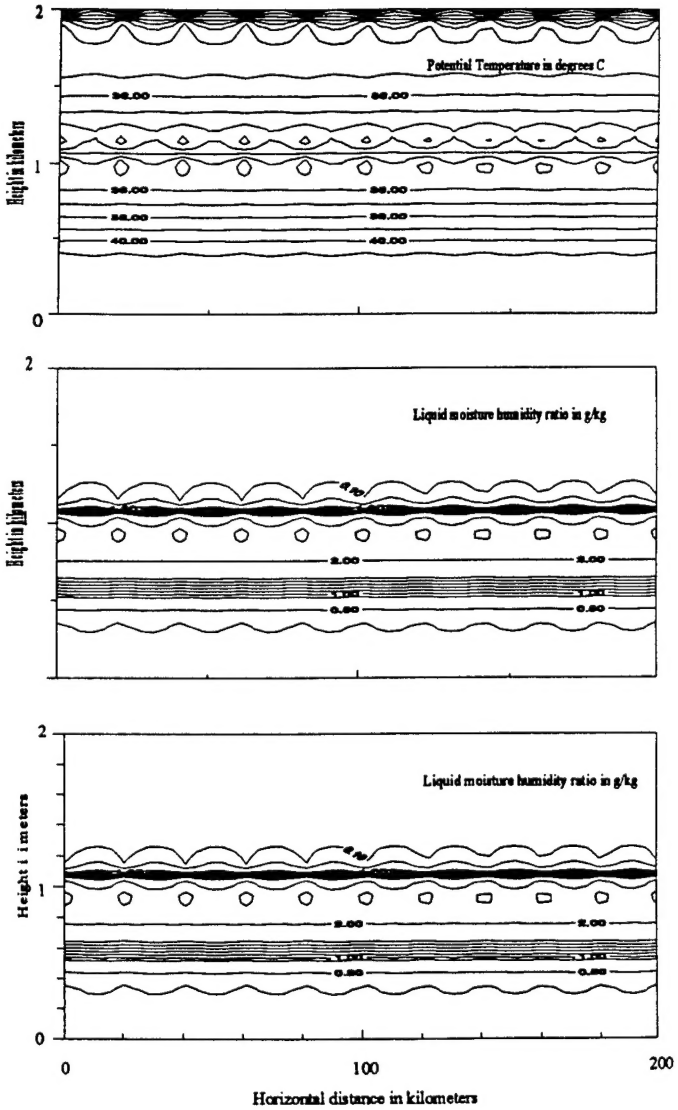

Fig. 4: Initial Steady state at the Zeroth Hour

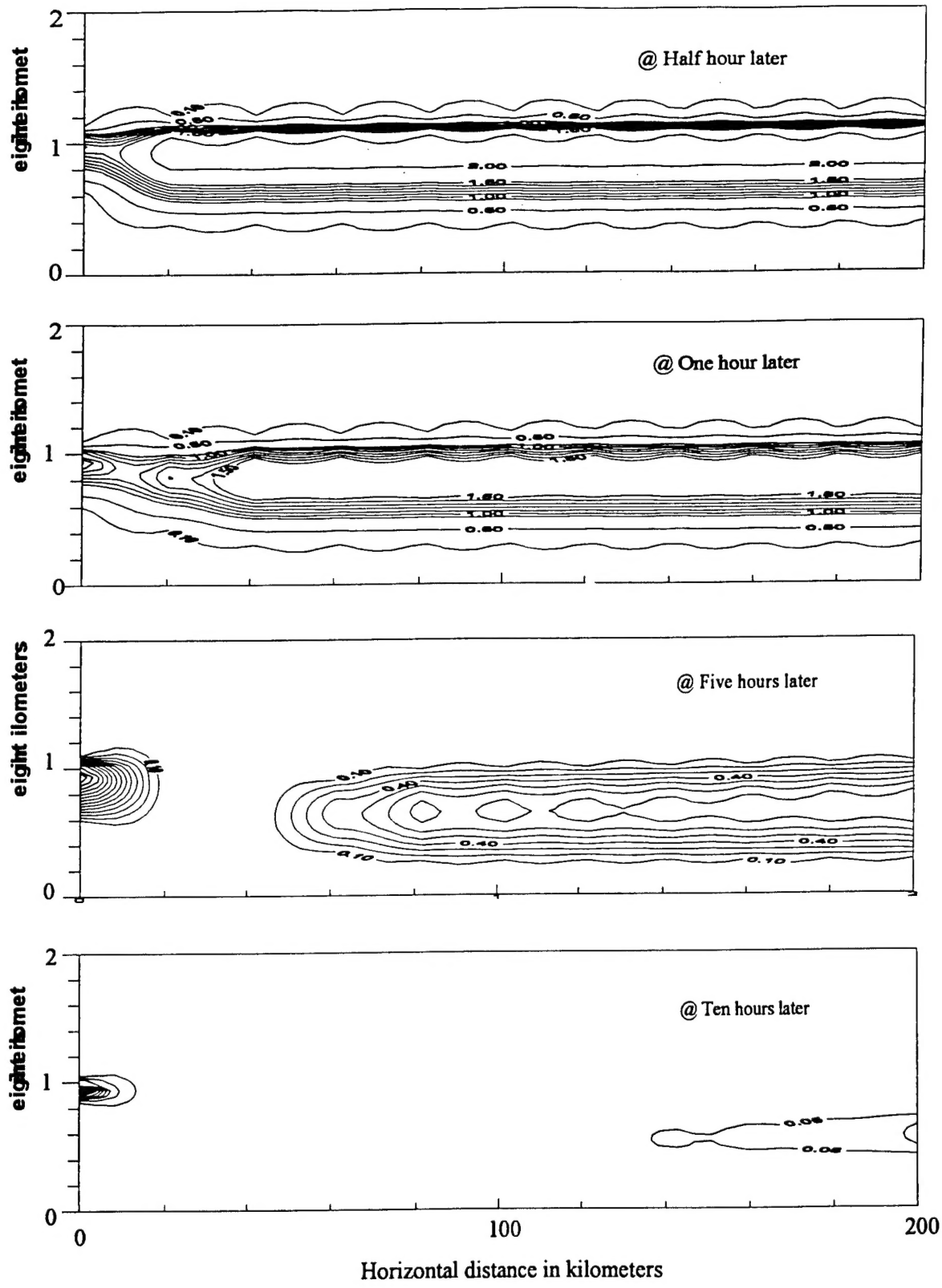

Fig. 5: Predicted Effects of Warm-Air Enrtrainment on the Cloud Stability (Plotted contours at different time are for liquid water humidity ratio values in grams per kilogram)

REPORT DOCUMENTATION PAGE

Form Approved
OMB No. 0704-0188

1. AGENCY USE ONLY *(Leave blank)*	2. REPORT DATE	3. REPORT TYPE AND DATES COVERED
	Dec. 15, 1998	Final Technical, 3/1/96 to 12/31/98

4. TITLE AND SUBTITLE

Dynamics of Marine Cloud Layers:
Computer Simulation and Experimental Verification

5. FUNDING NUMBERS

Grant Number:
N00014-96-1-0973

6. AUTHOR(S)

Joseph Chi, Ph.D., P.E.
Professor of Mechanical Engineering

7. PERFORMING ORGANIZATION NAMES(S) AND ADDRESS(ES)

University of the District of Columbia
4200 Connecticut Avenue, NW, MB4020
Washington, DC 20008-1174

8. PERFORMING ORGANIZATION REPORT NUMBER

UDC/ME/N973-05

9. SPONSORING / MONITORING AGENCY NAMES(S) AND ADDRESS(ES)

Office of Naval Research, Code 322MM
Ballston Centre Tower One
800 North Quincy Street
Arlington, VA 22217-5660

10. SPONSORING / MONITORING AGENCY REPORT NUMBER

11. SUPPLEMENTARY NOTES

a. DISTRIBUTION / AVAILABILITY STATEMENT

Defense Technical Information Center
8725 John J. Kingman Road, Suite 0944
Ft. Belvoir, VA 22060-6218

12. DISTRIBUTION CODE

13. ABSTRACT *(Maximum 200 words)*

Goals of this research have been to identify physical processes that determine the dynamics of marine cloud layers and to quantify roles of turbulence, convection and thermal radiation that play in formation, dissipation and stability of the marine cloud layers. And immediate objectives of the research are to advance turbulence models, use efficient numerical schemes, develop computer simulation programs, simulate the marine cloud layers and compare computer results with published experimental data on the marine cloud layers so as to yield insights into the cloud's physical processes.

For these objectives, two theoretical models, using the second-order-turbulence closure and the large-eddy simulation (LES), respectively, have been developed. In addition, a hybrid model has been presented: It uses a framework of multidimensional LES Model but uses turbulence intensity values calculated by unidimensional second-order-closure turbulence equations. Results of the computer simulation are compared with experimental data retrieved from reliable web-site sources.

14. SUBJECT TERMS	15. NUMBER OF PAGES
Marine meteorology, marine planetary boundary layer (MPBL), turbulence.cloud stability, computer simulation, second-order-closure model, LES, hybrid model.	57
	16. PRICE CODE

17. SECURITY CLASSIFICATION OF REPORT	18. SECURITY CLASSIFICATION OF THIS PAGE	19. SECURITY CLASSIFICATION OF ABSTRACT	20. LIMITATION OF ABSTRACT
None	None	None	None